

NASA TECHNICAL NOTE



NASA TN D-5155

NASA TN D-5155

DESIGN AND PERFORMANCE OF
TWO INTEGRATED CIRCUITS FOR
FLUIDIC-CONTROLLED PNEUMATIC
STEPPING-MOTOR SYSTEM

by Miles O. Dustin and Robert E. Wallhagen

Lewis Research Center

Cleveland, Ohio

DESIGN AND PERFORMANCE OF TWO INTEGRATED CIRCUITS FOR A
FLUIDIC-CONTROLLED PNEUMATIC STEPPING-MOTOR SYSTEM

By Miles O. Dustin and Robert E. Wallhagen

Lewis Research Center
Cleveland, Ohio

NATIONAL AERONAUTICS AND SPACE ADMINISTRATION

For sale by the Clearinghouse for Federal Scientific and Technical Information
Springfield, Virginia 22151 - CFSTI price \$3.00

ABSTRACT

The report describes the design, development, and testing of two integrated circuits for a fluidic-controlled pneumatic stepping-motor actuator system. Typical sizing calculations are demonstrated for determining the interconnecting line sizes. The integrated circuits control a nutator stepping motor up to 300 steps per second with a maximum output torque of 90 in. -lb (1020 cm-N) at zero speed.

DESIGN AND PERFORMANCE OF TWO INTEGRATED CIRCUITS FOR A FLUIDIC-CONTROLLED PNEUMATIC STEPPING-MOTOR SYSTEM

by Miles O. Dustin and Robert E. Wallhagen

Lewis Research Center

SUMMARY

This report describes the design, construction, and testing of two fluidic integrated circuits for the control of a pneumatic stepping-motor actuator system developed by the NASA Lewis Research Center. The circuit concepts were developed previously at Lewis and were evaluated with a breadboard model.

The fluidic elements of the first integrated circuit were photoetched into ceramic plates. These plates are stacked with a number of acrylic plastic plates to form the complete integrated circuit. The acrylic plates contain milled passages which interconnect the fluidic elements.

The second circuit consists of a stack of copper-alloy laminations. The fluidic elements and interconnecting passages are chemically etched into the laminations. The stack of laminations is fused together by diffusion bonding to form a solid block.

Both integrated circuits were evaluated on the stepping-motor actuator using the same fluidic power amplifiers built at Lewis. Curves of torque as a function of input pulse frequency were experimentally determined for both systems.

The power amplifiers used in this program were a modified version of those used in the breadboard system. The modifications, described in the report, were made to improve the pressure recovery from 40 to 55 percent.

Design steps are discussed, and sample calculations are included for determining the line sizes for proper impedance matching between fluidic elements of one of the integrated circuits.

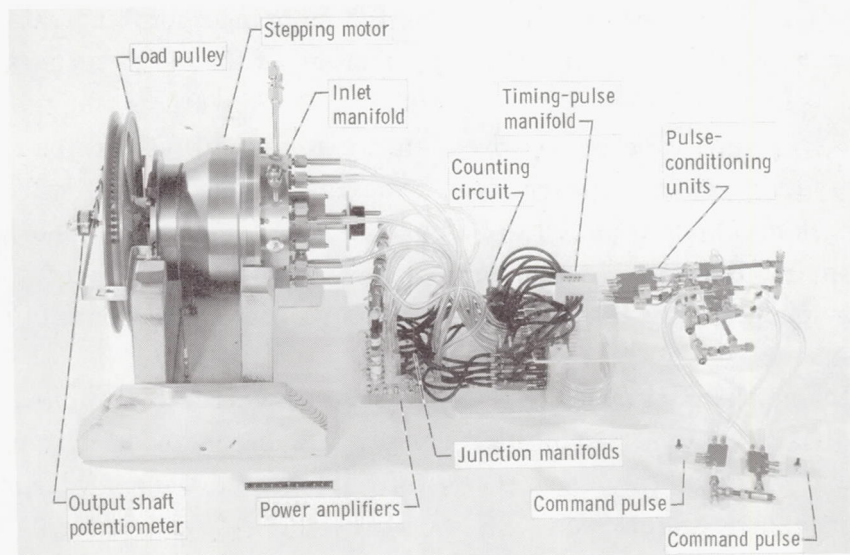
In this program, the performance of both integrated circuits matched or surpassed that of the breadboard system. From this result, it was concluded that an operational fluidic circuit can be completely and successfully integrated when a reasonably well-defined design procedure is followed.

INTRODUCTION

With the advent of nuclear reactors as power plants for rocket engines, some unique control problems arose. Performance requirements required that some of the critical control components be placed close to the nuclear reactor, which in turn necessitated that the components be highly insensitive to heat and radiation flux. One especially critical component is the actuator for the reactor control drums.

The nuclear rocket engine operates on high-pressure hydrogen, which provides a readily available source of power for a pneumatic actuator. However, pneumatic transmission delays require that the actuator controller be located near the actuator. An electronic control system would have remote logic but would still require a torque-motor-actuated pilot valve and feedback potentiometers located on the actuator. Thus, extreme cooling problems and questionable reliability of materials in the radiation field make the electronic control system far from ideal.

A potentially ideal system would be a high-speed fluidic control system mounted directly on a pneumatic actuator. Work toward the development of such a system has been done. A pneumatic stepping motor and a proportional fluidic control system were fabricated under contract to NASA. The stepping motor and control system are described in detail in reference 1. The response of this control system proved to be slower than required (ref. 1), and a new digital fluidic control system was developed at the NASA Lewis Research Center (ref. 2). This latter system, shown breadboarded with the stepping-motor actuator in figure 1, did meet the system response requirements.



C-66-3982

Figure 1. - Breadboard actuator system.

However, before any claims about the merit of this fluidic control system could be made, proof was needed that the complete circuit could be integrated into a compact module and mounted directly on the stepping-motor actuator.

Two integrated fluidic logic circuits were built, based on the design used in the breadboard circuit. Both circuits were evaluated with power amplifiers built by Lewis.

The first integrated circuit (designated A) was fabricated by Lewis, except for those portions that contained fluidic elements; these were designed by Lewis but were fabricated by Corning Glass Works. Corning's standard fluidic elements were used.

Except for the final-stage power amplifiers, the second integrated circuit (designated B) was fabricated by the Martin Marietta Corporation. The circuit design was modified by Martin to allow the use of standard Martin fluidic elements.

This report describes the design and developmental testing of both integrated circuits and also includes the design steps required to size correctly the interconnecting lines between elements in integrated circuit A.

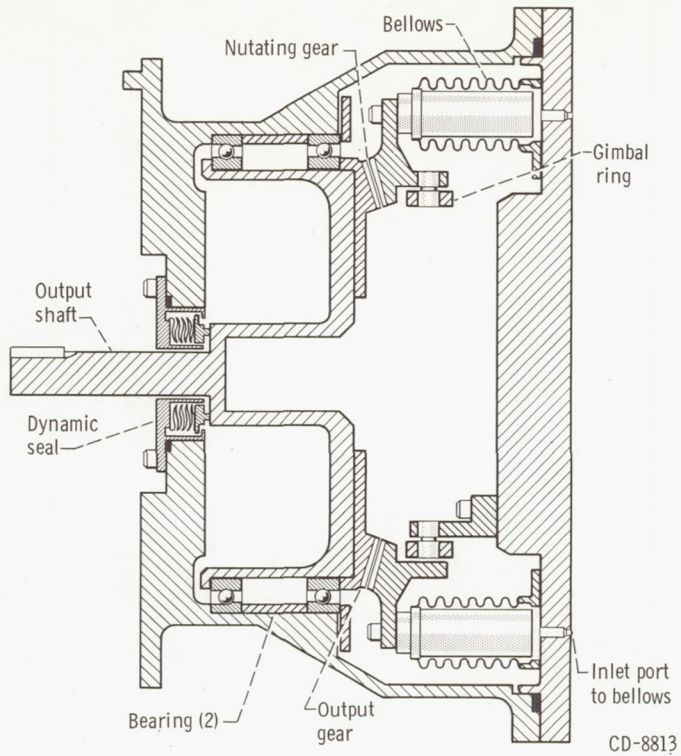
ACTUATOR SYSTEM DESCRIPTION

Actuator

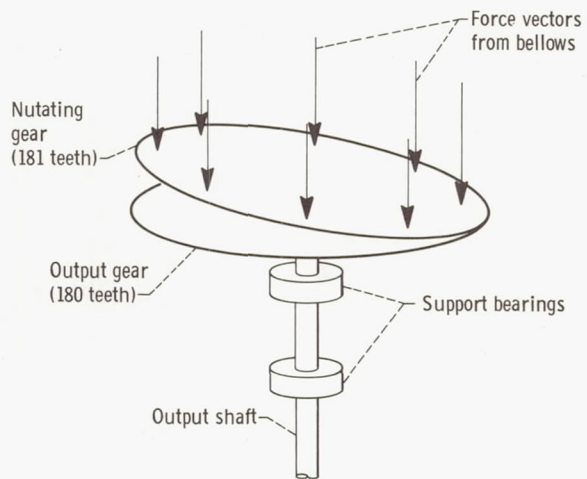
The pneumatic stepping motor used in the system (ref. 1) is shown in cross section in figure 2(a). The two basic parts of the actuator are an output gear, which is free to rotate only, and a nutating gear, which is free to nutate, or wobble, only. A simplified schematic diagram of the actuator is shown in figure 2(b). The nutating gear is controlled by eight bellows located around its periphery. When four adjacent bellows are pressurized, the nutating gear is tilted and forced into contact with the output gear. Sequencing the bellows pressurization pattern, as shown in figure 3, caused the nutating gear to nutate. The output gear is designed with 180 teeth and the nutating gear with 181, which causes the output gear to advance on tooth, or 2.0 degrees of rotation, for each complete cycle of the nutating gear. Figure 3 shows that one cycle of the nutating gear is composed of eight individual steps. Thus, for each step increment in the bellows pressurization pattern, the output gear rotates 0.25 degree.

Logic Circuit

The pressurization pattern for the actuator bellows is generated by a fluidic logic circuit developed at Lewis (ref. 2). The logic circuit with the actuator is shown in the block diagram of figure 4. This circuit consists of four subcircuits: two pulse-conditioning circuits, a counting circuit, and a power amplification circuit.



(a) Cross-sectional view.



(b) Schematic representation.

Figure 2. - Pneumatic stepping-motor actuator.

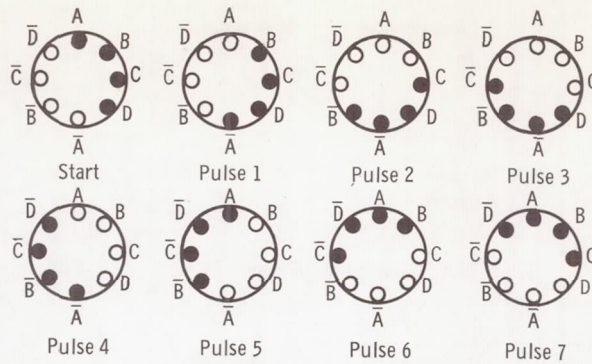


Figure 3. - Sequencing of bellows pressurization pattern by forward-counting input pulses.

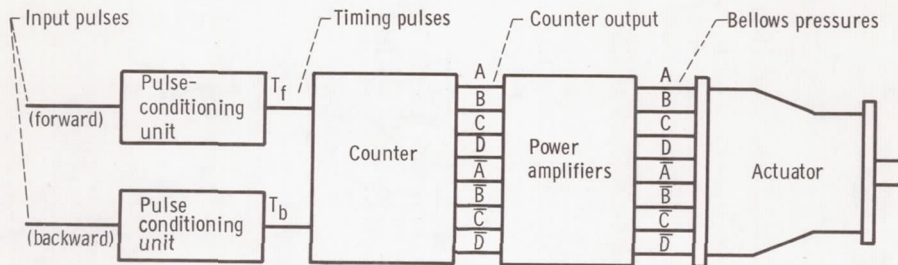


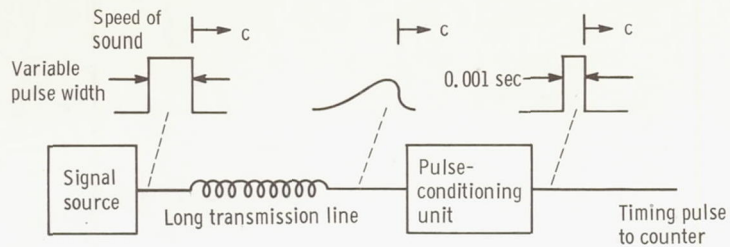
Figure 4. - Actuator system.

Pulse-conditioning circuit. - The input to the actuator system is a pneumatic pulse, which can be of variable width and may be considerably misshapen because of transmission-line effects, as depicted in figure 5(a). The desired input to the counting circuit is a squared pulse of 1 millisecond in duration. The schematic diagram of the pulse-conditioning circuit that performs the desired pulse shaping is shown in figure 5(b).

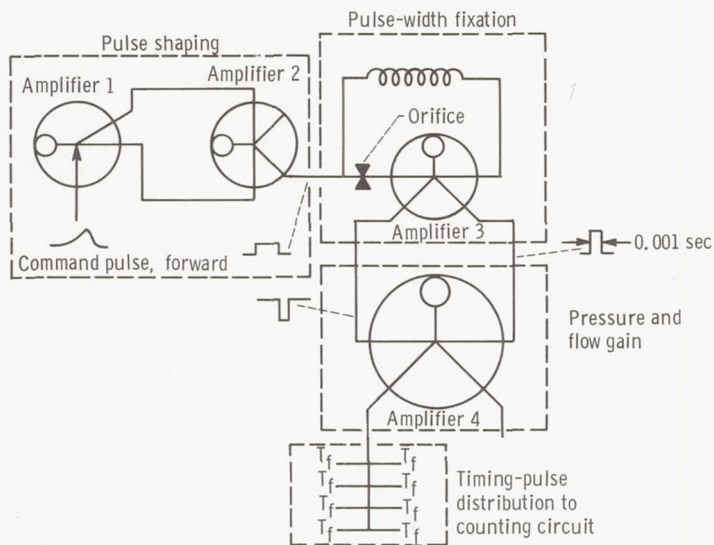
Amplifier 1 in figure 5(b) is an OR-NOR unit that converts the input pulse to a push-pull signal. This signal is then squarely shaped by the following bistable unit (amplifier 2). The pulse-width fixation unit is the critical part of the pulse-conditioning circuit. Amplifier 3 is a fixed one-shot multivibrator with a 1-millisecond output pulse width. This pulse is then further amplified in amplifier 4.

Two identical pulse-conditioning circuits are used: one shapes the command input (timing) pulses for forward actuator motion, and the other shapes the input pulses for backward actuator motion.

Counting circuit. - The purpose of the counting circuit is to store the actuator bellows pressurization pattern and to sequence it in either a forward or backward direction, depending on the direction of the command input pulse. A ring-type counter composed of four stages is used to accomplish these functions. The outputs of the stages are labeled



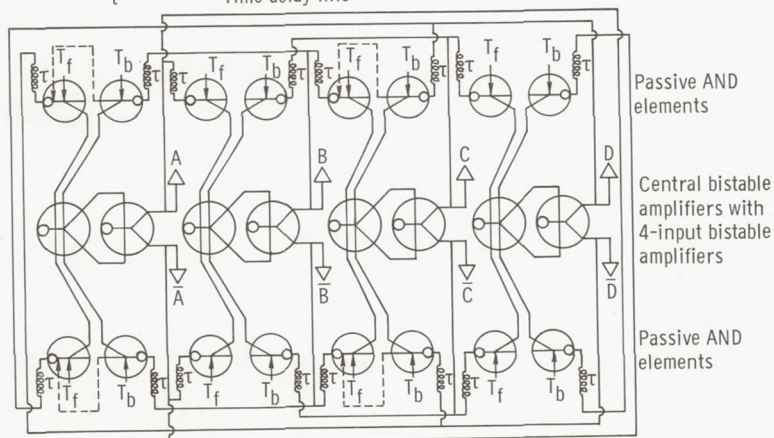
(a) Command pulse wave forms.



(b) Pulse-conditioning circuit.

Figure 5. - Pulse-conditioning unit.

A, \bar{A} ; B, \bar{B} ; Counting-circuit outputs (to control
 C, \bar{C} ; D, \bar{D} ; ports of power amplifier)
 T_b , Backward timing-pulse input ports
 T_f , Forward timing-pulse input ports
 τ Time delay line



CD-10140-03

Figure 6. - Counting circuit of integrated circuit A.

A, \bar{A} to D, \bar{D} , and they correspond directly to the actuator bellows positions indicated in figure 3. The schematic diagram for the complete counting circuit is shown in figure 6.

The forward command pulse from the forward pulse-conditioning circuit enters the counting circuit at eight locations marked T_f . Likewise, the backward pulse enters at eight locations marked T_b . (Symbols are defined in appendix A.) A rigorous description of the sequence of operation can be obtained in reference 2. The counting circuit of the breadboard system (ref. 2) used two separate dual-input OR-NOR units as control inputs to the center bistable amplifiers of each of the four stages. Just prior to the designing of integrated circuit A, a commercially available four-input bistable amplifier was introduced which replaced the two dual-input OR-NOR units. The modified schematic diagram of the complete counting circuit used in integrated circuit A (fig. 6) shows the four-input bistable amplifier used as the input to the central bistable amplifier.

Power amplifiers. - A power amplification stage is required to boost the outputs of the central bistable amplifiers in the counting circuit to a level where they can drive the nutating gear in the stepping motor. A supersonic bistable amplifier, described in reference 2, was used for this purpose in the breadboard system.

The recovered pressures from the outputs of the power amplifiers are applied directly to the actuator bellows and determine the output torque at which the output gear of the stepping motor disengages from the nutating gear. Increasing the output torque of the system required redesigning the power amplifiers to increase their pressure recovery. A description of the redesigned amplifier is given in the section Integrated Circuit A Design.

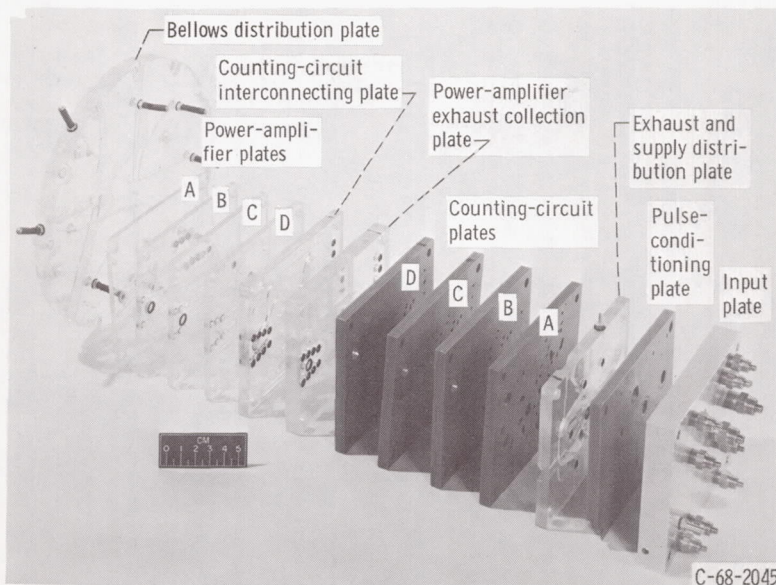


Figure 7. - Stack of plates comprising integrated circuit A.

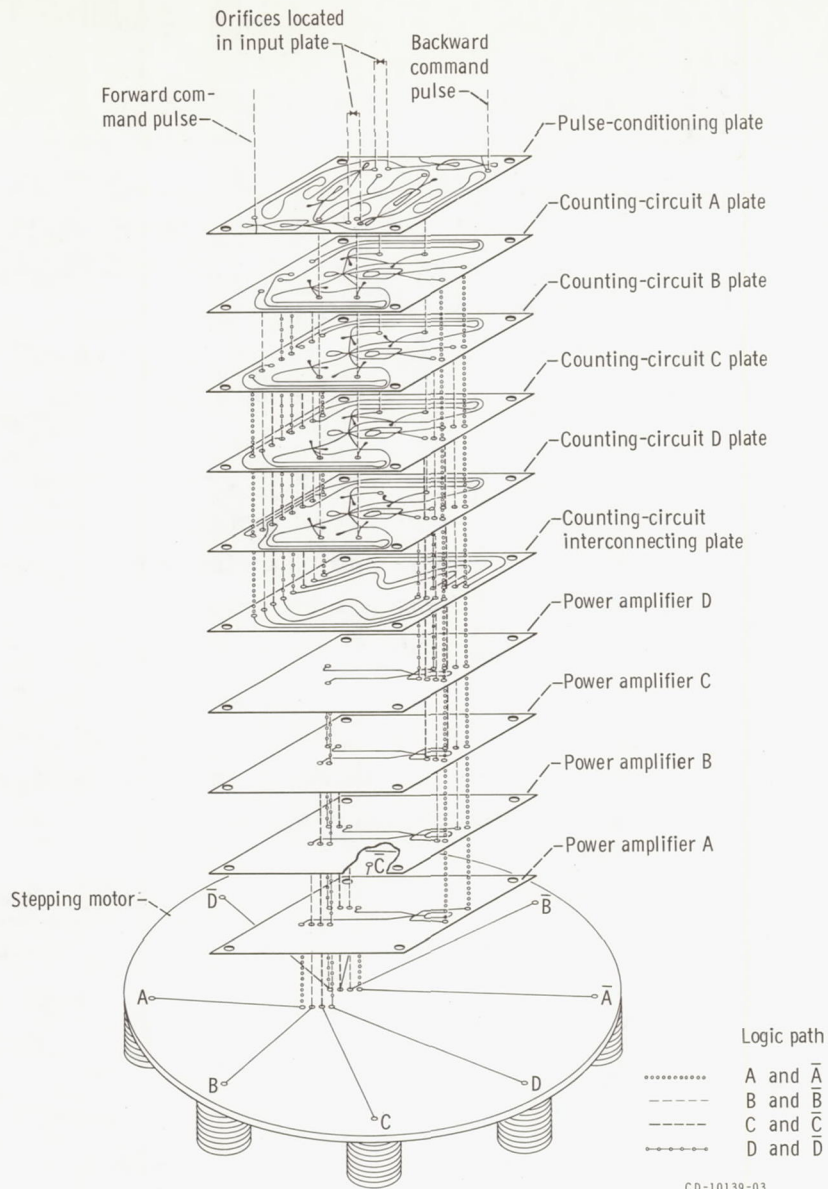


Figure 8. - Expanded schematic diagram of integrated circuit A.

INTEGRATED CIRCUIT A

Integrated Circuit A Design

Integrated circuit A consists of a stack of plates, shown in the photograph of figure 7. One of these plates contains the two pulse-conditioning circuits; four plates contain the counting circuit; and separate plates each contain one of the four power amplifiers. Other plates in the stack contain interconnecting channels between individual amplifier circuits and provide supply passages and exhaust vents. An expanded schematic representation of the integrated circuit is shown in figure 8. For simplicity, only those plates containing fluidic devices plus the counting-circuit interconnecting plate are shown. The complete integrated circuit detached from the stepping motor is shown in figure 9. This circuit was designed to allow easy disassembly for testing individual circuit plates.

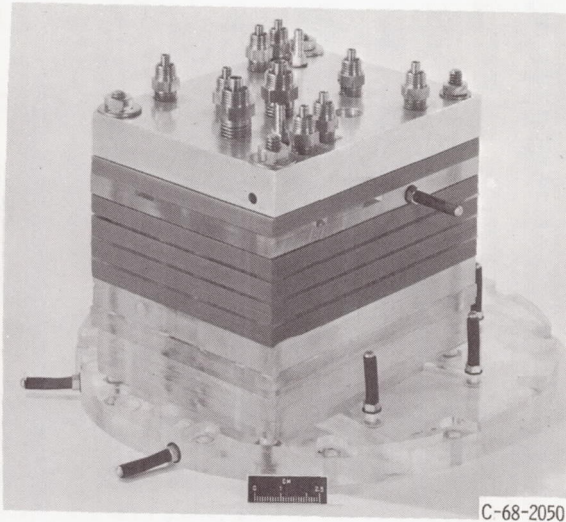
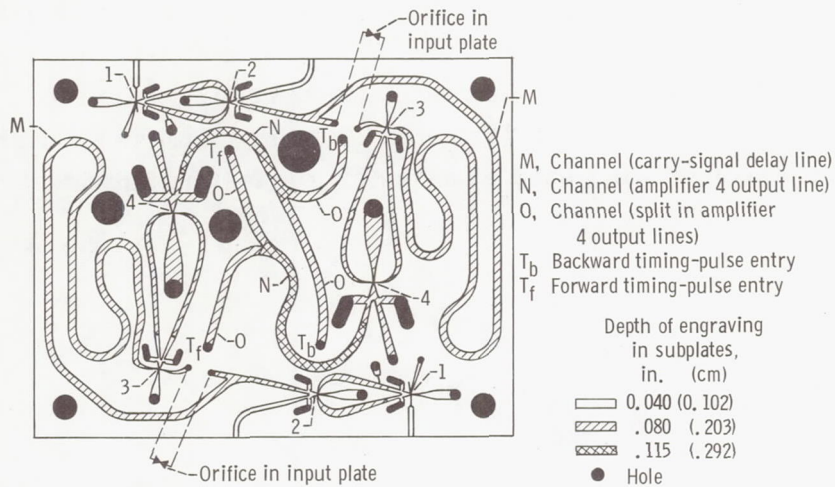


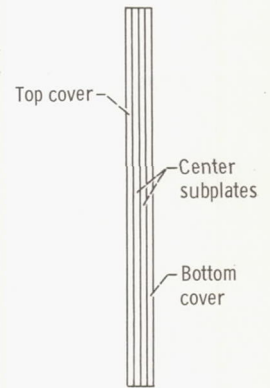
Figure 9. - Integrated circuit A mounted on power amplifiers and bellows distribution plate.

The plates containing the pulse-conditioning circuits and the counting circuit were fabricated from a photoetched ceramic. The interconnecting manifolds and power amplifier plates were fabricated by milling passages into acrylic plastic sheets. The input plate for the supply and input pulse connections was aluminum. The complete stacked assembly was bolted to a bellows distribution plate which in turn was mounted on the stepping-motor backplate. Rubber O-rings were used as seals between plates.

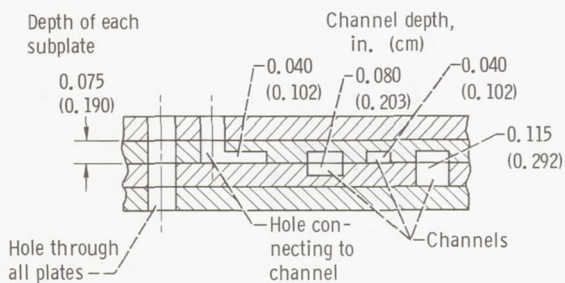
Pulse-conditioning-circuit plate. - The pulse-conditioning-circuit engraving pattern and the engraving depths are shown in figure 10. The plate consists of four 0.075-inch (0.19-cm) thick subplates. The pattern shown in this figure is engraved in the facing



(a) Engraving pattern on plate of pulse-conditioning circuit.



(b) End view of subplates.



(c) Representative section illustrating method used to obtain different engraving depths.

CD-10141-03

Figure 10. - Pulse-conditioning-circuit-plate engraving pattern for integrated circuit A.

surfaces of the two center subplates. Areas engraved 0.040 inch (0.10 cm) deep are in only one center subplate. Areas that are 0.080 inch (0.20 cm) deep are engraved 0.040 inch (0.10 cm) deep in the facing surfaces of both center subplates. The 0.115-inch (0.292-cm) deep engraving is 0.040 inch (0.10 cm) deep in one center subplate and through the other. Supply holes, vents, and interconnecting ports are engraved through the cover plates.

The delay-line channel (channel M in fig. 10) connecting the output of amplifier 2 to the input of amplifier 3 was sized to deliver a pulse with a single reflection back to amplifier 2. The technique for determining the proper channel size is described fully in appendixes B and C of reference 2. The single-reflection line permits one to use larger lines than would be used if the line were acoustically matched to the control port of amplifier 3. A line sized by the single-reflection technique delivers a pulse shape identical to that delivered by an acoustically matched line. However, the friction losses are lower because of the larger line size. The required area for these channels was calculated to be 0.0062 square inch (0.040 cm²). The channel dimensions were 0.080 inch (0.20 cm) deep by 0.077 inch (0.19 cm) wide. The calculations for determination of these line sizes are given in appendix B.

The output lines of amplifiers 4, which are the timing pulses to the inputs of the counting circuit, were also sized to give a pulse with a single reflection back from the counting circuit inputs T_f and T_b . The output lines of amplifiers 4 split to provide timing pulses to both sides of each counting-circuit block. At the outputs of amplifier 4, the channel (labeled N in fig. 10) has a cross-sectional area of 0.015 square inch (0.096 cm²), or 0.130 inch (0.330 cm) wide by 0.115 inch (0.292 cm) deep. After the split, the channel (labeled O in fig. 10) has a cross-sectional area one-half that of channel N or 0.0075 square inch (0.048 cm²). The dimensions of channel O are 0.094 inch (0.239 cm) wide by 0.080 inch (0.203 cm) deep. The channel-sizing calculations are given in appendix B.

The pulse-conditioning-circuit plate was designed so that the orifices at the inputs of amplifiers 3 could be changed. The orifices are located in the top plate adjacent to the proper porting holes in the pulse-conditioning plate. The orifice porting arrangement is shown schematically by the dashed lines in figure 10.

Engineering and performance data and supply pressures for the elements used in the pulse-conditioning circuit are listed in table I.

Counting-circuit plate. - Engraved patterns for the four counting-circuit plates are shown in figure 11.

Each counting-circuit plate is composed of one central bistable amplifier, its associated four-input bistable amplifier, and four passive AND elements.

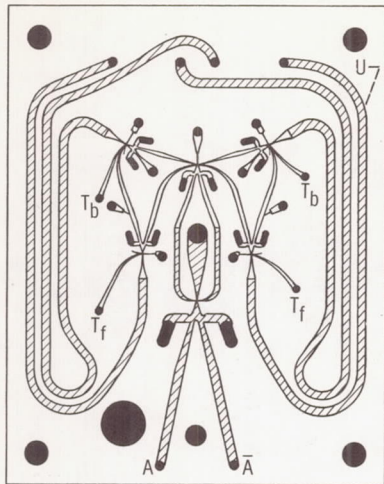
The counting circuit plates were engraved to two depths, as shown in figure 11. These plates were also fabricated of four 0.075-inch (0.19-cm) subplates, and the

TABLE I. - PERFORMANCE AND ENGINEERING DATA AND SUPPLY PRESSURES

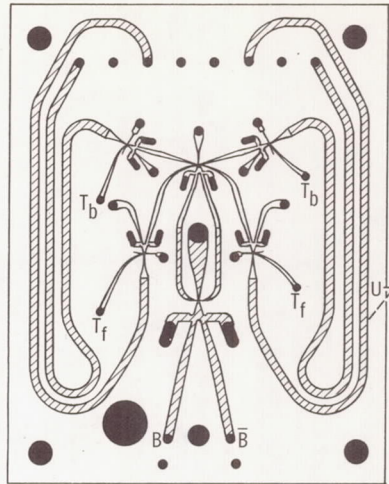
FOR FLUIDIC AMPLIFIERS USED IN INTEGRATED CIRCUIT A

Amplifier		Nozzle size								Supply pressure, $P_s - P_e$		Maximum pressure recovery, percent of supply
Location	Type	Power				Control				psig	N/cm ² gage	
		Width	Depth	Width	Depth	Width	Depth	Width	Depth			
		in.	in.	cm	cm	in.	in.	cm	cm			
Pulse-conditioning circuit												
1	Wall attachment, OR-NOR gate	0.010	0.040	0.025	0.100	(a)	(a)	(a)	(a)	4.0	2.8	35
2	Wall attachment, bistable	.010	.040	.025	.100	0.010	0.040	0.025	0.100	4.0	2.8	33
3	Wall attachment, bistable	.010	.040	.025	.100	.010	.040	.025	.100	4.0	2.8	33
4	Wall attachment, bistable	.020	.080	.050	.200	.020	.080	.050	.200	10.0	6.90	33
Counting circuit												
Passive AND	Wall attachment, OR-NOR gate	0.010	0.040	0.025	0.100	(a)	(a)	(a)	(a)	(b)	(b)	35
Four-input bistable	Wall attachment, bistable	.010	.040	.025	.100	(a)	(a)	(a)	(a)	12.0	8.28	33
Central bistable	Wall attachment, bistable	.020	.080	.050	.200	0.020	0.080	0.050	0.200	12.0	8.28	33
Power-amplifier stage												
Lewis supersonic power amplifier	Wall attachment, bistable	0.040	0.060	0.100	0.150	(c)	(c)	(c)	(c)	45.0	31.0	55

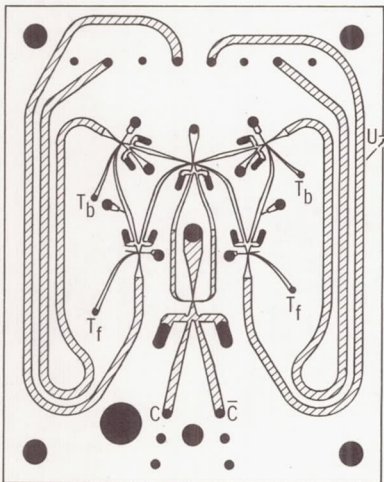
^aNot available from manufacturer.^bNo supply (passive element).^cNot defined (see fig. 12(a)).



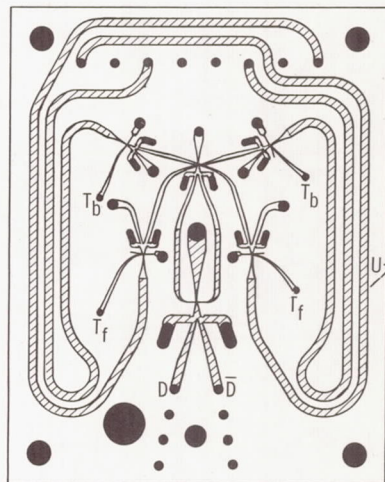
(a) Plate A.



(b) Plate B.



(c) Plate C.



(d) Plate D.

Engraving depths

— 0.040 (0.102)

▨ .080 (.203)

● Hole

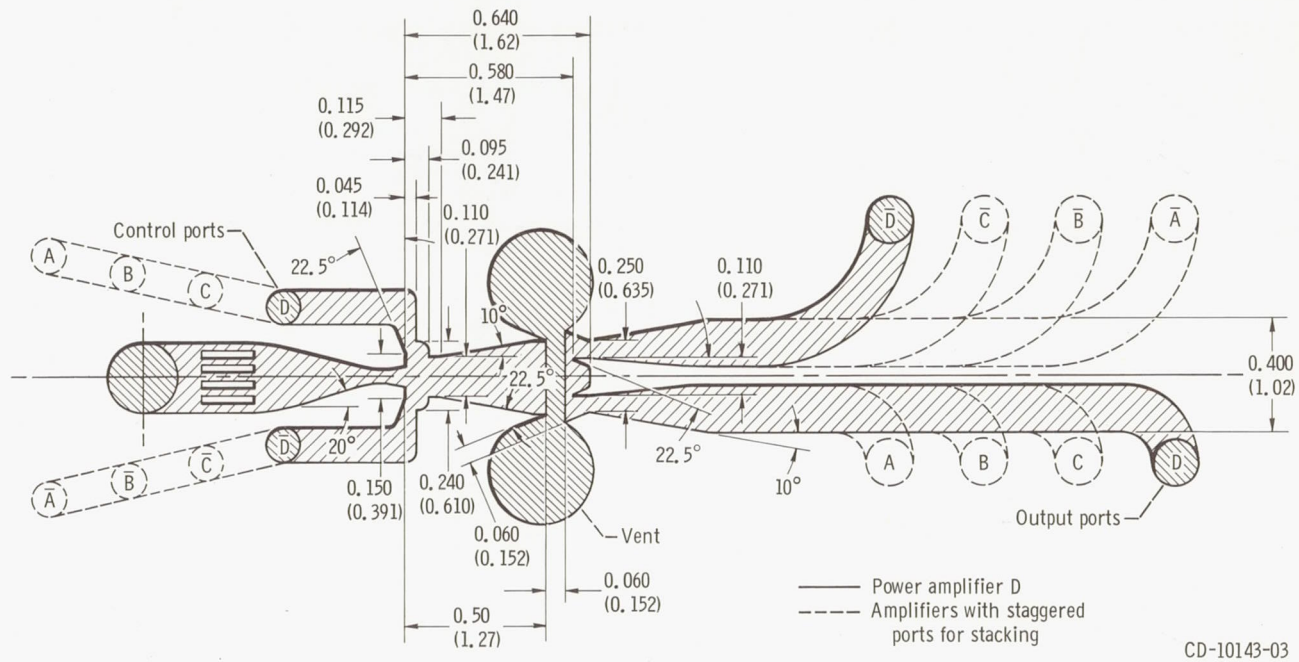
A, \bar{A} ; B, \bar{B} ; Amplifier outputs CD-10142-03

C, \bar{C} ; D, \bar{D}

T_b , T_f Forward timing-pulse input parts

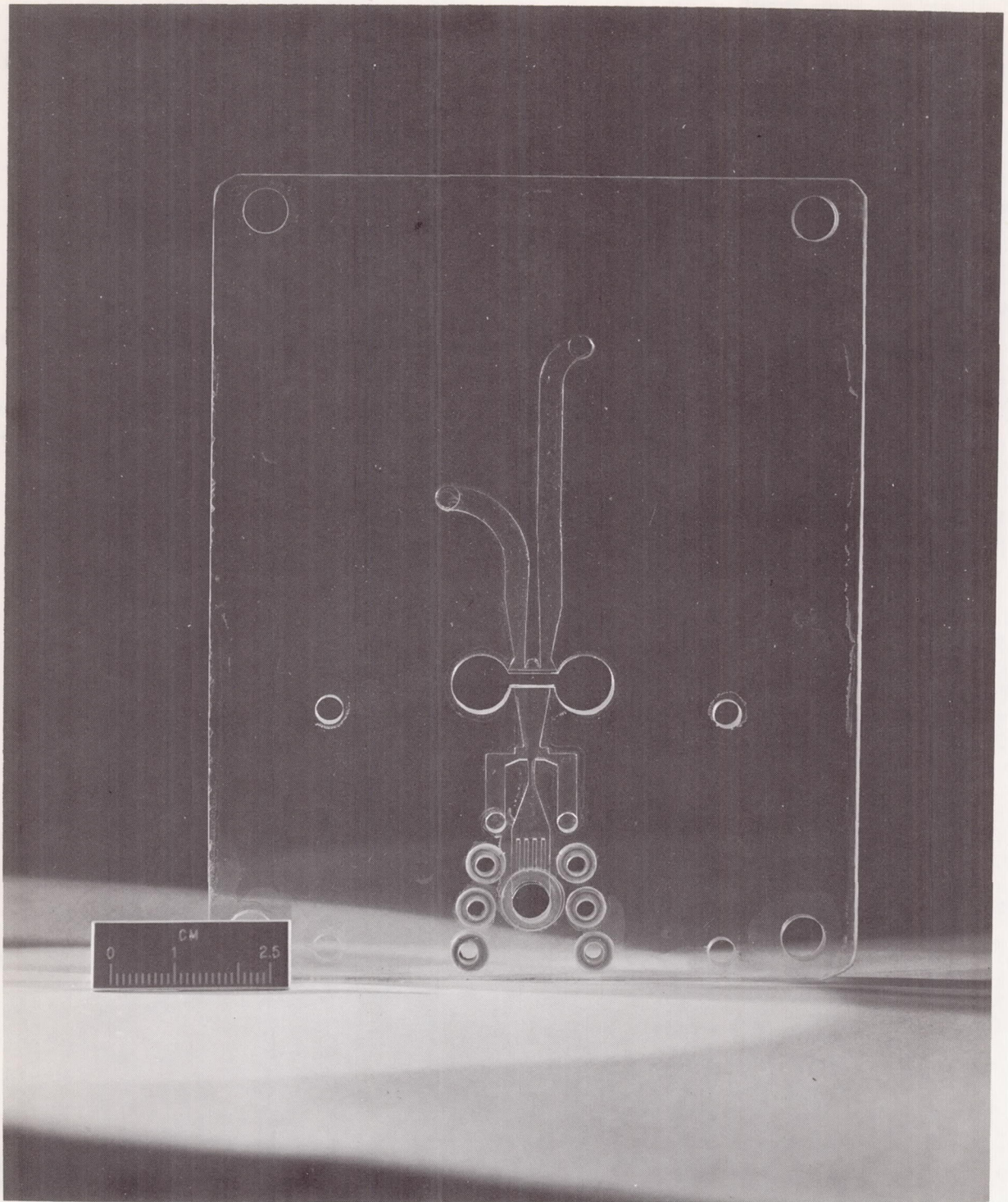
U Channel (carry-signal delay line)

Figure 11. - Counting-circuit-plate engraving patterns and depths for integrated circuit A. (All dimensions are in in. (cm).)



(a) Engraving pattern. Depth of engraving (except for vents), 0.060 inch (0.153 cm); Mach 1.63 nozzle (throat, 0.04 in. (0.102 cm)). All dimensions are in inches (cm).

Figure 12. - Power amplifiers used in integrated circuits A and B.



(b) Power amplifier D.
Figure 12. - Concluded.

method used to obtain the different engraved depths was the same as that used for the pulse-conditioning plates.

The carry-signal delay lines, which feed the passive AND elements (identified as channel U in fig. 11); were sized by the single-reflection technique. The areas of these channels as calculated in appendix B were 0.00785 square inch (0.0506 cm²), or 0.098 inch (0.249 cm) wide by 0.080 inch (0.203 cm) deep.

Engineering and performance data and supply pressures for the elements used in the counting circuit are listed in table I.

Power amplifiers. - The SB1 power amplifiers, designed by Lewis and used in the breadboard stepping-motor actuator system, were redesigned to obtain a greater pressure recovery. An increase in pressure recovery from 40 to 55 percent was achieved. A drawing of the redesigned amplifier, with the important dimensions, is shown in figure 12(a). The major changes in the new power amplifier were the reduction of the side-wall angle from 20° to 10°, the elimination of the center vent, and the elimination of two side-wall vents. The drawing (fig. 12(a)) shows the control inputs from the counting circuit, labeled A, \bar{A} to D, \bar{D} and the similarly labeled outputs that are fed directly to the actuator bellows. The photograph of figure 12(b) shows power amplifier D, which amplifies the D and \bar{D} outputs of the counting circuit.

The power amplifiers were engraved in a 0.125-inch- (0.317-cm-) thick acrylic plastic sheet with a 0.062-inch- (0.157-cm-) thick cover plate.

Counting-circuit interconnecting plate. - The counting-circuit interconnecting plate is located between the power-amplifier exhaust collection plate and the power amplifiers. The interconnecting plate is shown in the photograph of figure 13.

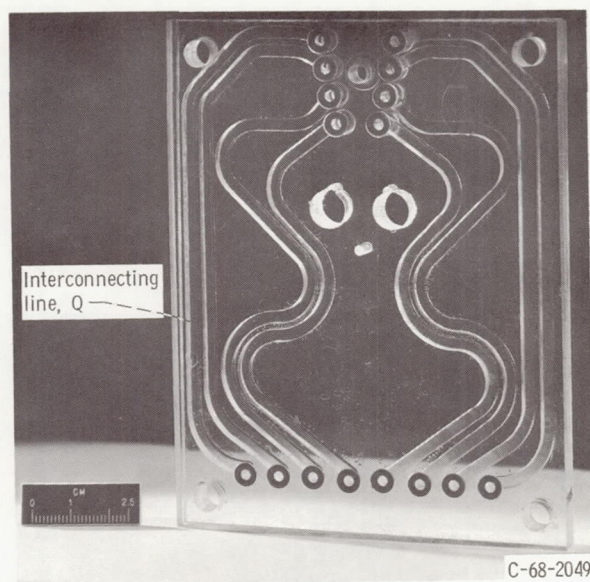


Figure 13. - Counting-circuit interconnecting plate for integrated circuit A.

The counting-circuit interconnecting plate connects the outputs of the central bistable amplifiers with the power nozzles of the passive AND elements in the counting-circuit plates. The length of the interconnecting lines Q in this plate plus the length of the lines to the AND elements in the counting-circuit plates create a time delay. This delay allows the 1-millisecond timing pulse to decay before the counting circuit is reset. This combined length is about 20 inches (50 cm). The area of each of the interconnecting lines, calculated in appendix B, is 0.0157 square inch (0.101 cm²). The line dimensions are 0.125 inch (0.318 cm) wide by 0.125 inch (0.318 cm) deep. The plate was fabricated by milling the channels into one acrylic plastic sheet and then cementing it to a second sealing sheet.

Exhaust and supply distribution plate. - The exhaust and supply distribution plate shown in figure 14 collects the exhaust from the amplifier vents of both the counting cir-

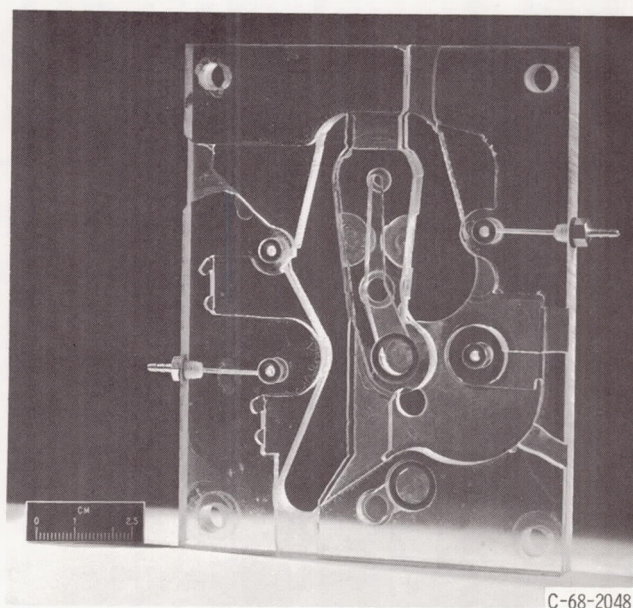


Figure 14. - Exhaust and supply distribution plate for integrated circuit A.

cuit and the pulse-conditioning circuit. The exhaust exits to atmosphere directly from the exhaust and supply distribution plate and through an exhaust passage through the input plate. The exhaust cavity in the exhaust and supply distribution plate is also connected internally to the exhaust cavity in the power-amplifier exhaust collection plate. The exhaust and supply distribution plate also distributes the supply flows to the counting-circuit active elements and directs the supply flow to the power amplifiers.

Bellows distribution plate. - The bellows distribution plate is located between the power amplifiers and the stepping motor. It receives the outputs from the power amplifiers and distributes them to the bellows of the actuator. It also collects half of the

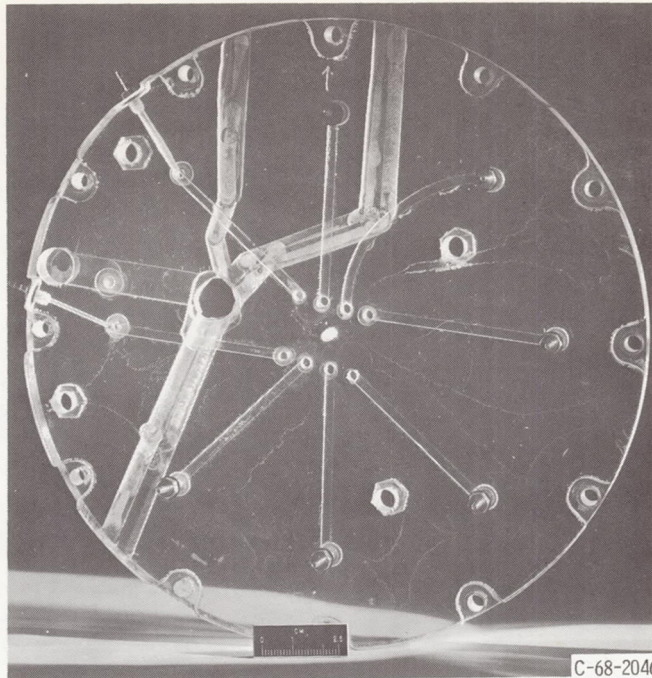


Figure 15. - Bellows distribution plate used with integrated circuits A and B.

power-amplifier exhaust flow and ports it to the outside ambient air. The bellows distribution plate is shown in the photograph of figure 15.

The plate was fabricated by milling channels into an acrylic plastic sheet and sealing with a second acrylic plastic sheet. The channels are 0.125 inch (0.318 cm) wide by 0.098 inch (0.249 cm) deep. The optimum channel area was determined experimentally by applying step pressure changes to a tube with a volume termination. The volume size was the same as that of the bellows used in the motor. Various line diameters were tested to determine the diameter that resulted in the smallest time constant. The volume pressure was measured with a quartz piezoelectric-type transducer. A 0.125-inch (0.318-cm) inside diameter tube was determined to be the optimum size. An area equivalent to a 0.125-inch- (0.318-cm-) diameter tube was used for the channels in the bellows distribution plate.

Integrated Circuit A Test Results and Discussion

Pulse-conditioning-circuit testing. - The pulse-conditioning circuit was tested separately to verify the 1-millisecond pulse width of its output. Command input pulses of various widths were fed to the pulse-conditioning circuit and the output was monitored.

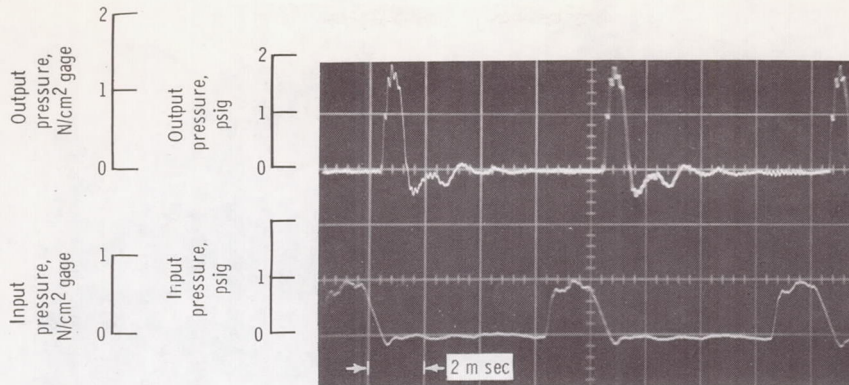


Figure 16. - Integrated circuit A pulse-conditioning-circuit input and output wave forms. Pulse rate, 120 pulses per second.

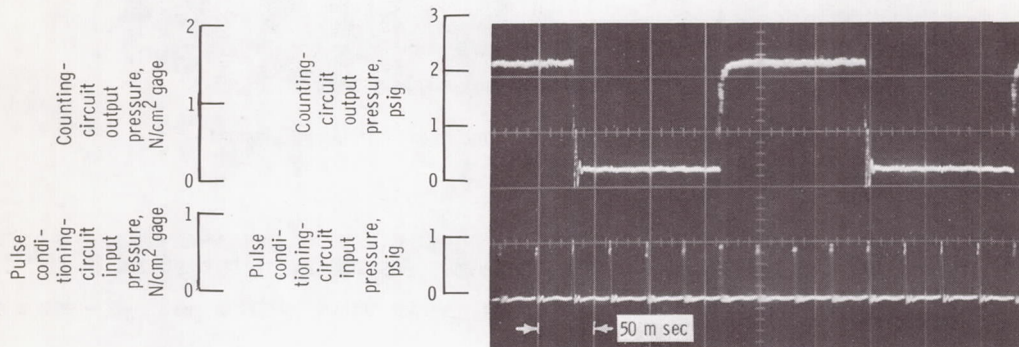


Figure 17. - Integrated circuit A counting-circuit output pressure responding to system input pulses. Pulse rate, 30 pulses per second (circuit not matched to control port impedance of power amplifier).

An oscilloscope tracing of a typical input and output pulse shape is shown in figure 16. The pulse-conditioning-circuit output (upper tracing) is the desired 1-millisecond pulse width.

Counting-circuit testing. - The counting circuit was run in conjunction with the pulse-conditioning circuit to determine whether or not the counter advanced the bellows pressurization pattern properly. For proper functioning of the systems, the output of each central bistable amplifier in the counting circuit should switch once for every four input pulses. The oscilloscope tracing shown in figure 17 demonstrates that a typical counting-circuit output (upper tracing) does switch on every fourth input pulse (lower tracing). A visual check was made to verify that the counting circuit maintained four adjacent bellows locations pressurized at all times.

Complete integrated circuit testing. - The complete stepping-motor actuator system with integrated circuit A, is shown installed on the test bench in figure 18. The system is instrumented to run dynamic-response measurements. The dynamic-response tests were conducted by driving the actuator system with eight pulses in the forward direction

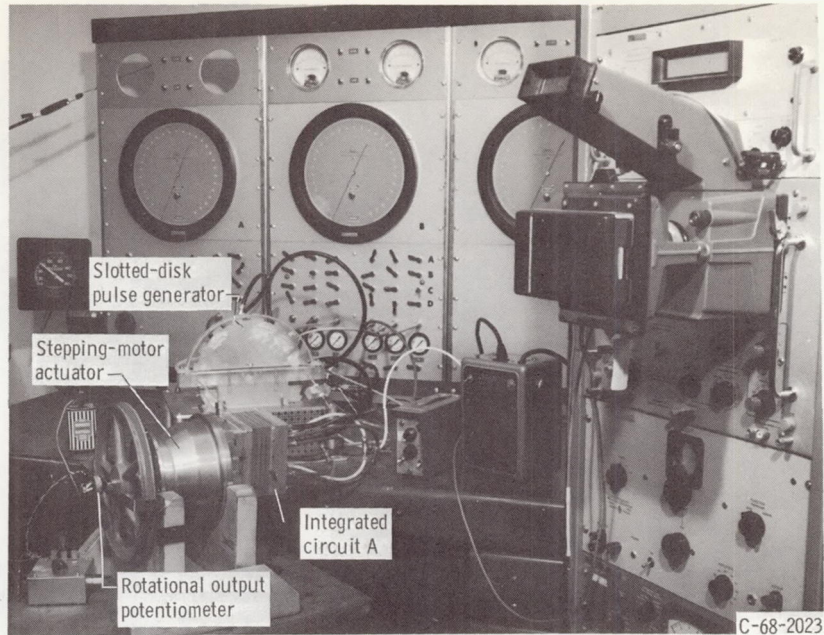


Figure 18. - Complete actuator system using integrated circuit A instrumented for dynamic-response measurements.

and then with eight pulses in the reverse direction. As the actuator steps 0.25° for each input pulse, the output of the actuator was a triangular wave with a peak-to-peak amplitude of 2° .

The output of the actuator was monitored through a rotational potentiometer. Oscilloscope tracings of the output are shown in figure 19. As the pulse rate is increased, the inertia of the output wheel, combined with possible play in the keyway and in the actuator gears, filters out the discrete stepping motion of the output tracing.

The tracing in figure 19(e) was run at 300 pulses per second, which is considerably higher than the maximum speed obtained from the breadboard stepping-motor actuator system. In fact, the integrated stepping actuator system A was run successfully to 360 pulses per second. In reference 2, Griffin concluded that the speed limitation of the motor was primarily the result of the bellows time constant. This time constant is determined by the bellows and line volumes and the restriction hole in the actuator back plate. During the breadboard testing, these restriction holes were 0.040 inch (0.10 cm) in diameter. Before the integrated circuit was run, these holes were drilled out to 0.125 inch (0.318 cm) in diameter, which matched the line size and essentially removed the restriction. Also, the integrated circuit reduced the line volume to the bellows from the power amplifiers. Higher power-amplifier pressure recovery also reduced the time required for the bellows to reach the pressure that was obtained in the breadboard system.

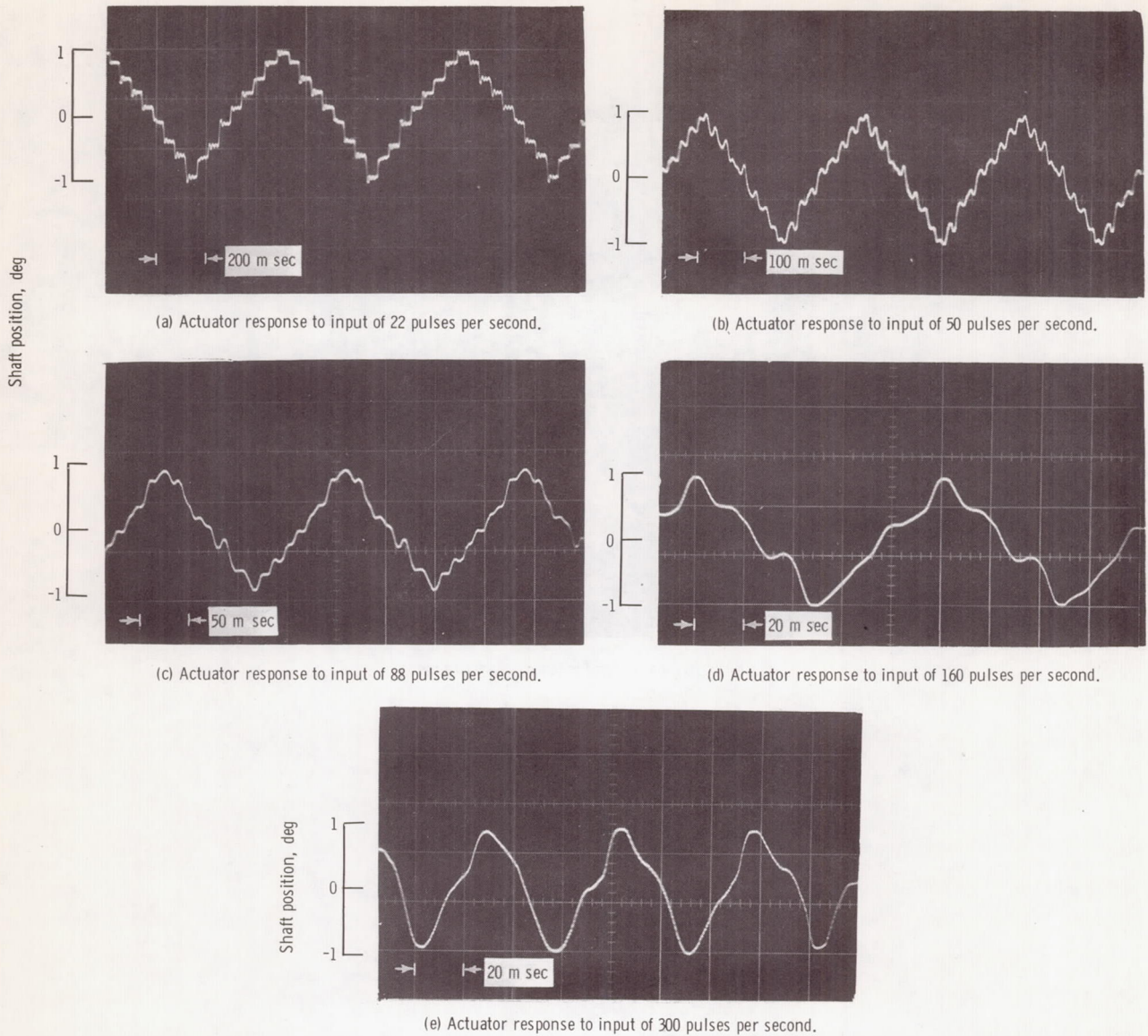
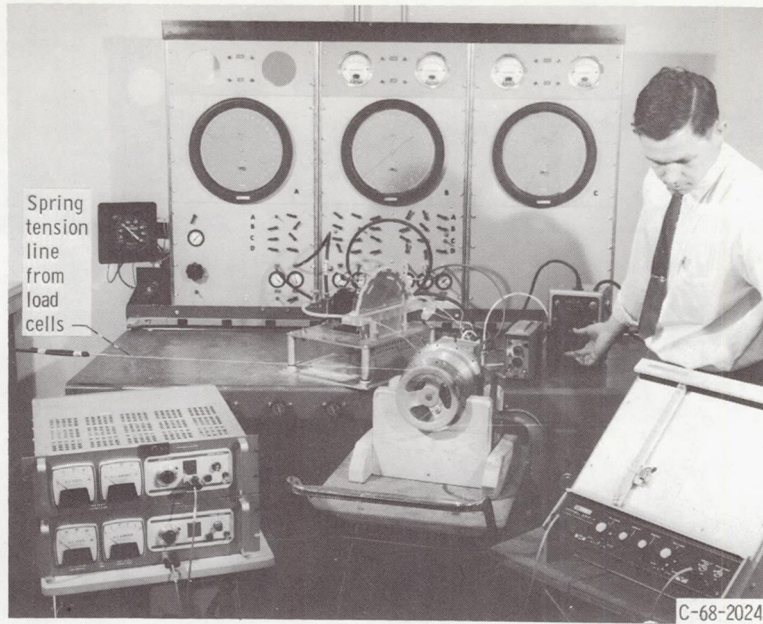
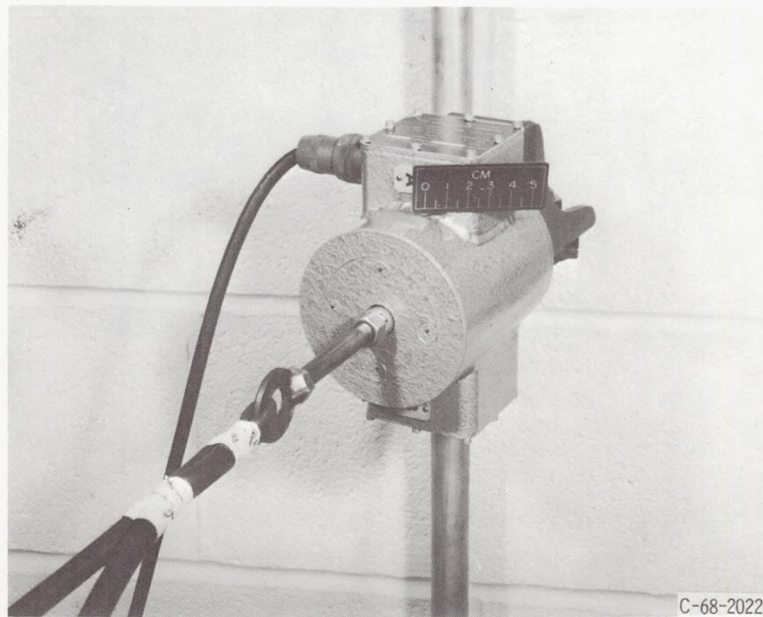


Figure 19. - Output response of actuator system using integrated circuit A. Input pulse alternated between forward and backward input ports after every eighth input pulse.

As is shown later in this section, the output torque of the actuator motor does not fall to zero, even at 300 input pulses per second. From the output torque curve, the limiting factor in the system does not appear to be the bellows charging time. Now, the carry-signal delay time is the limiting factor. This carry-signal delay time consists of the switching times of the four-input bistable and the central bistable amplifiers plus the transit time for the total line length in the feedback loop. The longest total line length is approximately 21.5 inches (54.6 cm), which causes a transit delay time of 1.6 milliseconds. Assuming a switching time of 0.5 millisecond for each of the two amplifiers in



(a) Instrumentation for torque measurements.



(b) One of load cells used in making torque measurements.

Figure 20. - Complete actuator system using integrated circuit A.

the loop gives a total carry-signal delay time of 2.6 milliseconds. This time delay would limit the maximum frequency to 385 pulses per second.

The output torque of the actuator system was determined by connecting two large rubber springs between the actuator output wheel and two load cells. The instrumentation layout on the test bench is shown in figure 20. The moment arm that the load spring works through was 2.75 inches (7.0 cm). The output of the load cells was calibrated as a function of the load force and converted into the torque applied to the actuator. Total actuator torque was monitored directly on an X, Y-recorder.

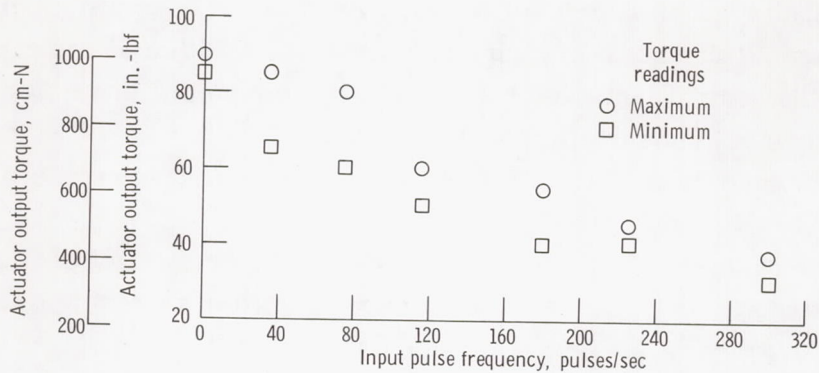


Figure 21. - Output torque as function of input pulse frequency for actuator system using integrated circuit A.

A plot of output torque as a function of input pulse frequency is shown in figure 21. The actuator was run at constant speed, and the torque was read when the actuator gears disengaged. The rather large band on the curve of output torque as a function of input pulse frequency is probably the result of minute variations in the actuator gears. As the load is increased on the actuator output wheel, it becomes increasingly harder for the bellows to force the nutating gear into perfect mesh with the output gear. If the location of one bellows pressurization pattern fails to seat the nutating gear properly, and, hence, not fully increment the output gear 0.25° , the next location of the bellows pressurization pattern must force its portion of the nutating gear into the output gear at a larger offset. The larger offset in the tooth alignment yields a larger contact angle at the tooth contact line and makes it still harder to mesh the two gears. Thus, as soon as one portion of the nutating gear fails to seat properly, continued motion of the actuator causes the nutating gear to climb out of engagement completely. The torque at which this occurs can vary depending on small imperfections in the gear teeth or on dirt particles interfering with the meshing of the gears.

INTEGRATED CIRCUIT B

Integrated Circuit B Description

Counting circuit. - A schematic diagram of the integrated circuit B counting circuit, shown in figure 22, is a modified version of the original design used in integrated circuit A (fig. 6). The modifications allowed the contractor to use his standard amplifier configurations. The primary modifications were (1) the addition of two stages of amplification between the passive AND elements, and the central bistable amplifier group, accomplished with OR-NOR elements, (2) the use of three bistable amplifiers in the central bistable amplifier group instead of the four-input bistable amplifier and the large central bistable amplifier shown in figure 6, and (3) the addition of two stages of amplification between the central bistable group and the power amplifiers. For simplification, these two stages are not shown in figure 22.

Additional information on the amplifiers used in the counting circuit along with the supply pressures are listed in table II.

Delay lines were not used in this circuit. However, because of the number of fluidic elements in the circuit, there was enough delay in amplifier switching times so that the

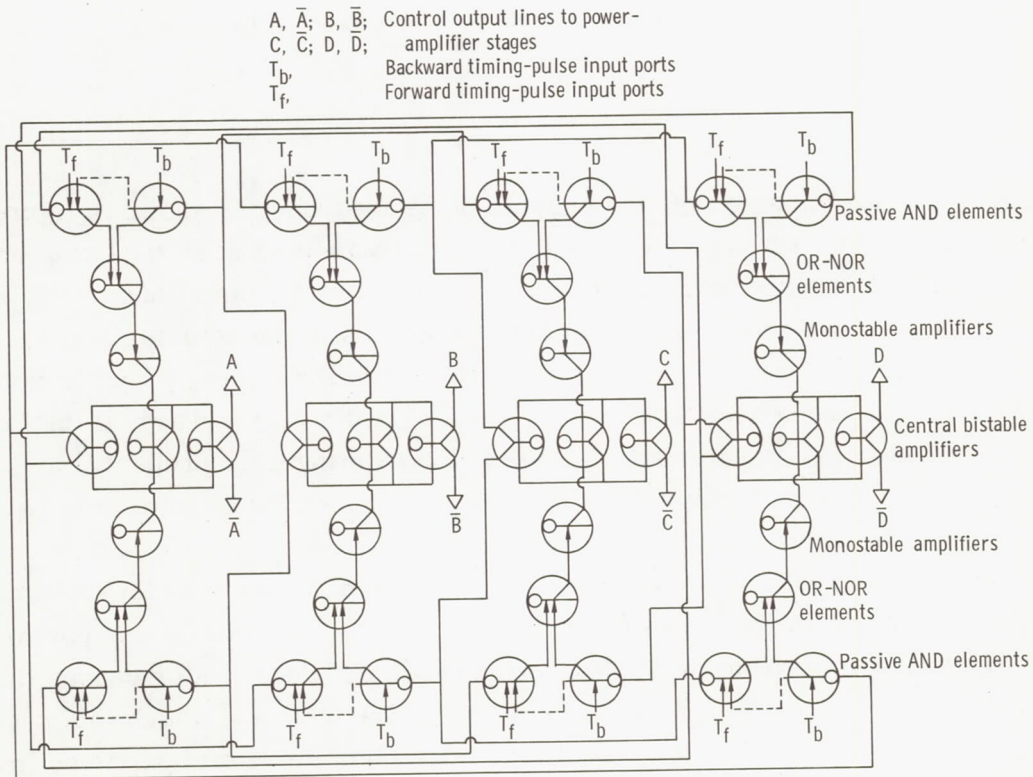


Figure 22. - Counting circuit of integrated circuit B.

CD-10144-03

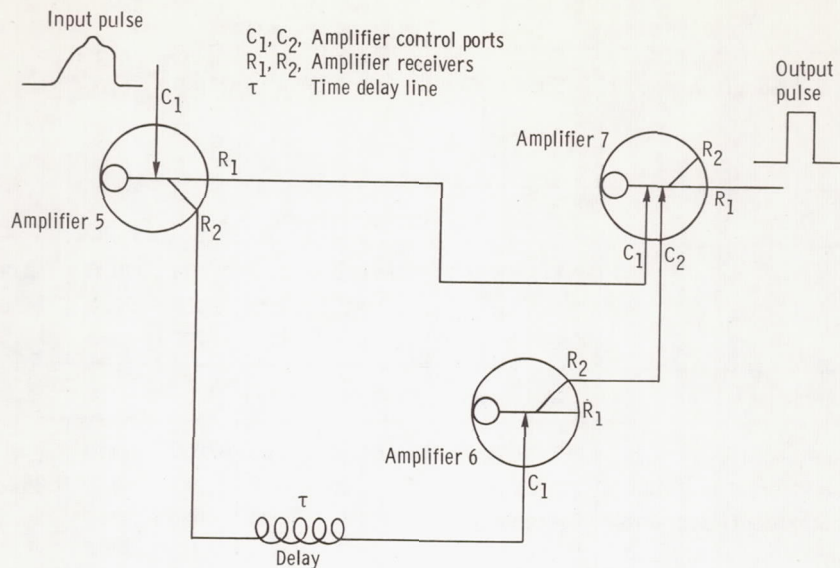


Figure 23. - Pulse-conditioning circuit of integrated circuit B.

counting circuit would not reset until the input pulse was terminated.

Pulse-conditioning circuit. - The pulse-conditioning circuit for integrated circuit B used a different arrangement of elements to obtain pulse-width fixation than that used by integrated circuit A. Three OR-NOR elements were used in each of the pulse-conditioning circuits, as shown in figure 23. In the normal condition, when the circuit input is zero, the output of amplifier 5 is directed out of receiver R_1 , which is connected to control port C_1 of amplifier 7. Amplifier 7 is thus switched to its output receiver R_2 . When an input pulse is applied to the control port C_1 of amplifier 5, amplifier 5 switches from its output receiver R_1 , which allows amplifier 7 to switch to its output receiver R_1 . The circuit output pulse is now switched on. The output pulse is terminated when the output receiver R_2 of amplifier 5 switches amplifier 6 to its output receiver R_2 , which in turn switches amplifier 7 to its output receiver R_2 . The output pulse width from receiver R_1 of amplifier 7 is determined by the length of the delay line between amplifiers 5 and 6. The delay time is approximately 0.5 millisecond, which is a short enough time to cause the timing pulse to be terminated before the carry signals of the counting circuit have reset the counting circuit for the next pulse.

Engineering data and supply pressures for the pulse-conditioning circuit-amplifiers are listed in table II.

TABLE II. - ENGINEERING DATA AND SUPPLY PRESSURES FOR
FLUIDIC AMPLIFIERS USED IN INTEGRATED CIRCUIT B

Amplifier		Size of power nozzle				Supply pressure, $P_s - P_e$	
Location	Type	Width	Depth	Width	Depth		
		in.	in.	cm	cm	psig	N/cm ² gage
Pulse-conditioning circuit							
5	OR-NOR	0.010	0.010	0.025	0.025	20.0	13.8
6	OR-NOR	.010	.010	.025	.025	20.0	13.8
7	OR-NOR	.010	.010	.025	.025	38.0	26.2
Counting circuit							
Passive AND	OR-NOR	0.010	0.010	0.025	0.025	(a)	(a)
Left central bistable	Bistable	.015	.015	.038	.038	38.0	26.2
Center central bistable	Bistable	.010	.010	.025	.025	38.0	26.2
Right central bistable	Bistable	↓	↓	↓	↓	38.0	26.2
Single-input OR-NOR	OR-NOR	↓	↓	↓	↓	20.0	13.8
Double-input OR-NOR	OR-NOR	↓	↓	↓	↓	9.5	6.5

^aNo supply (passive element).

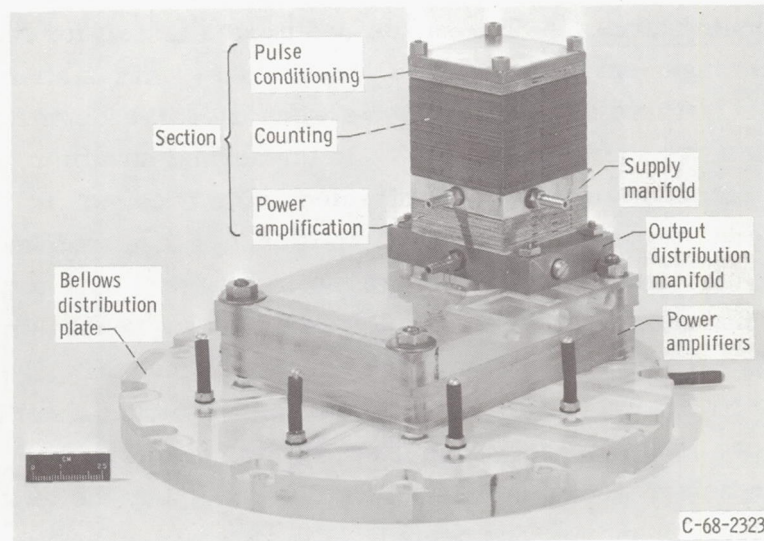
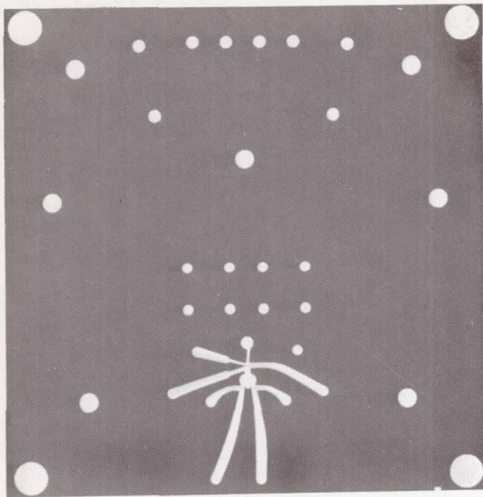
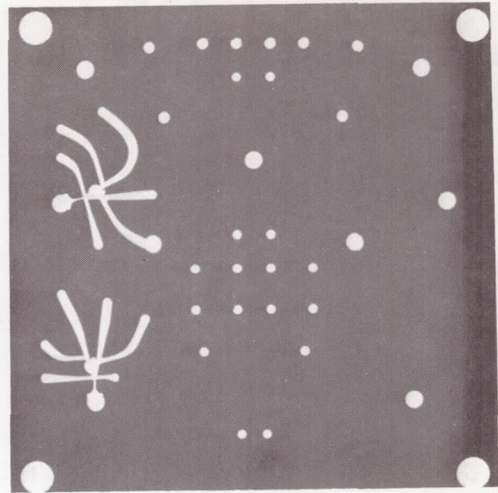


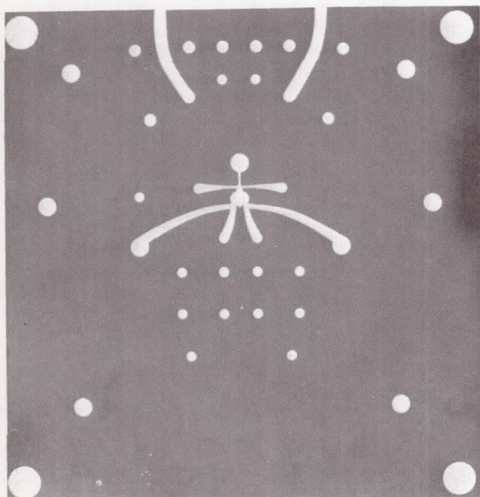
Figure 24. - Integrated circuit B mounted on power amplifiers and bellows distribution plate.



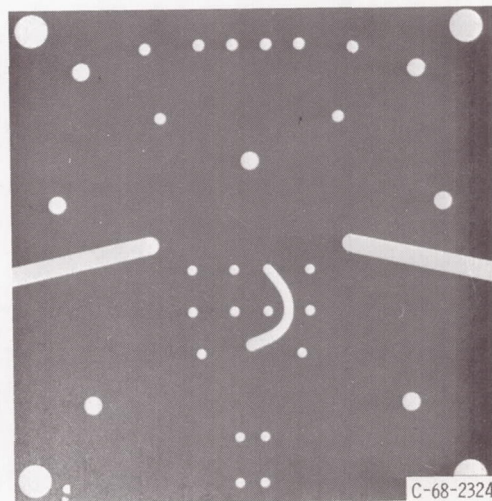
(a) OR-NOR element.



(b) OR-NOR elements.



(c) Bistable amplifier.



(d) Interconnecting plate.

Figure 25. - Typical laminations used in integrated circuit B.

Integrated Circuit B Design

Integrated circuit B is shown in the photograph of figure 24. The individual fluidic elements are chemically etched in thin copper-alloy laminations. Several typical laminations are shown in figure 25. Interconnections between fluidic elements are made by additional etched laminations (fig. 25(d)). The laminations are stacked and fused together by diffusion bonding.

The assembled integrated circuit in figure 24 consists of three bonded sections: (1) the pulse-conditioning section, (2) the counting section, and (3) the power amplification section. The power amplification section is required to amplify the counting circuits output pressure and flow to values high enough to switch the Lewis designed power amplifiers. The three sections are bolted to a supply manifold and an output distribution manifold to form the complete logic portion of the system.

Integrated Circuit B Test Results and Discussion

The integrated circuit B logic module, including the pulse-conditioning units, the counting-circuit stages, and preliminary power amplification stages, was tested by the Martin Company prior to contract completion. Further tests on that portion of the complete circuit were deemed unnecessary.

The complete stepping-motor actuator system with integrated circuit B, was tested in a manner identical to that previously described in the section Integrated Circuit A Test Results and Discussion.

Oscilloscope tracings of the output of the actuator system are shown in figure 26 for eight input pulses alternately applied in the forward and backward directions. These tracings were made at speeds that closely matched those used in integrated circuit A system test (fig. 19).

A difference in input pulse frequencies resulted because the speed of the input pulse generator could not be set precisely. The integrated circuit B system did respond to input pulse rates higher than 300 pulses per second, but the performance was not reliable enough to photograph.

An output torque test was run on the integrated circuit B system, and the curve was essentially the same as that for integrated circuit A. This output torque curve is plotted in figure 27. The curve is expected to match the torque curve of integrated circuit A (fig. 21) because the final output amplifiers are the same and use the same supply pressure. These conditions yield static bellows pressures that are the same for both systems, and because the actuator motor torque is dependent on bellows pressure, the output torque of both systems should be equal.

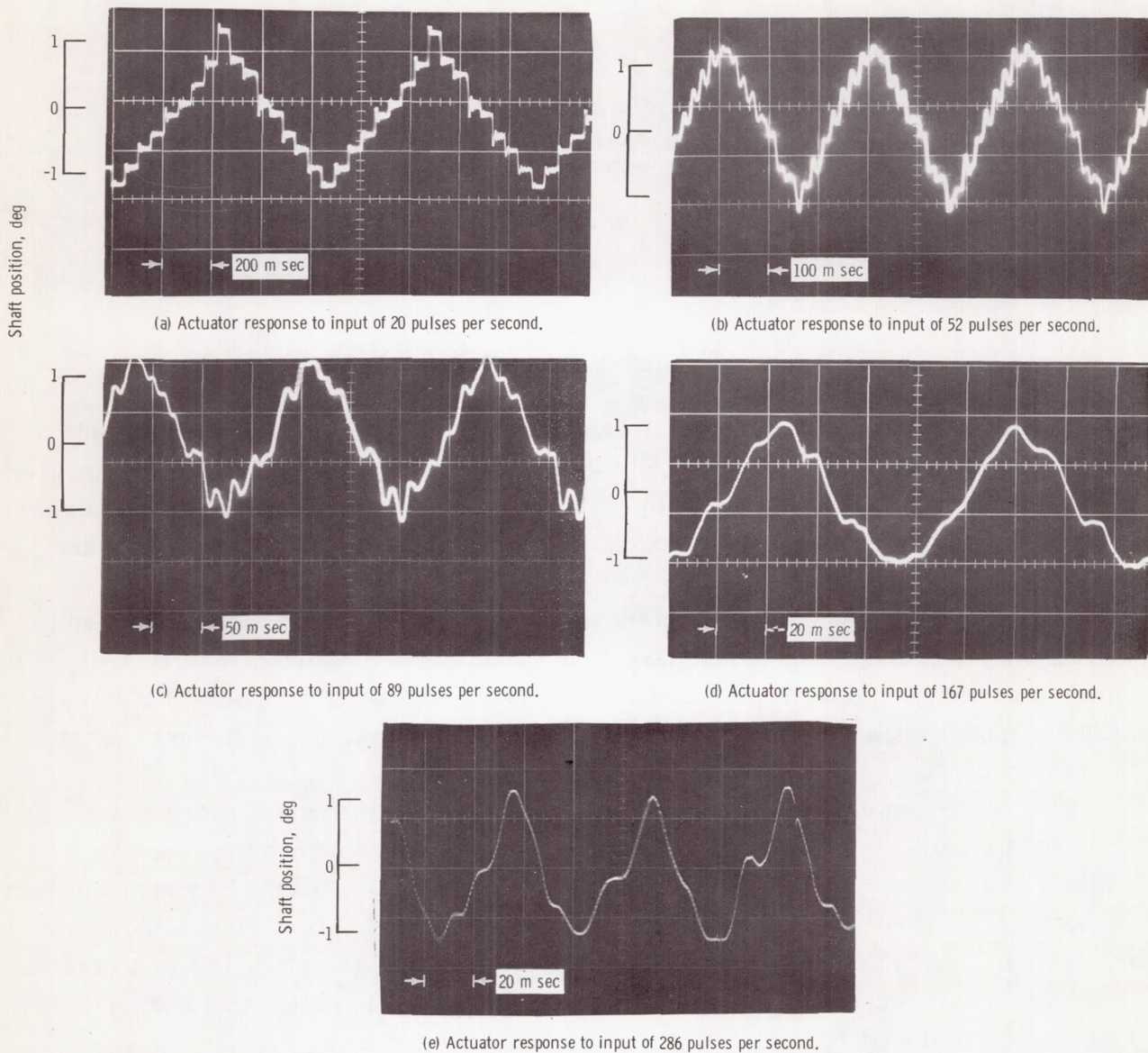


Figure 26. - Output response of actuator system using integrated circuit B. Input pulse alternated between forward and backward input ports after every eighth input pulse.

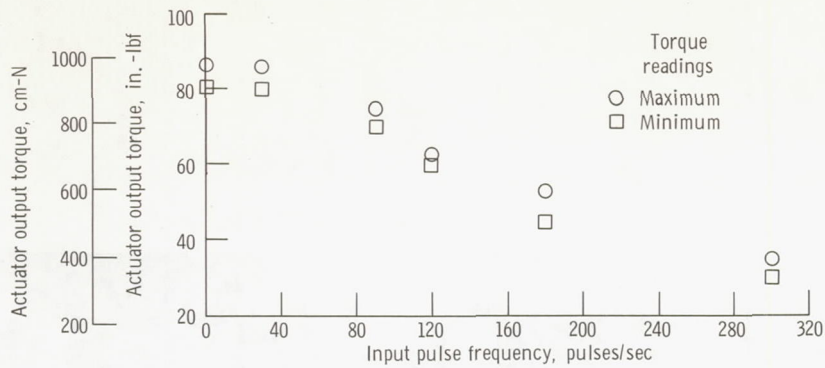


Figure 27. - Output torque as function of input pulse frequency for actuator system using integrated circuit B.

DISCUSSION

Stepping-Motor Actuator System Reliability

The results presented in the results and discussion section for both integrated circuit A and integrated circuit B are the best that were achieved. The interpretation given to these results should not be that both circuits are running with 100 percent reliability at the speeds and torque levels presented. The best results were presented because they represent the system potential.

The stepping-motor actuator system had more torque output at all speeds when it was running in a counter-clockwise direction with either integrated circuit controlling it. Whether or not this problem was inherent in the stepping-motor actuator or in the integrated circuits was not determined. The output torque curves presented were taken in the best direction.

Both integrated circuit systems failed to react to all input pulses consistently. Both appeared to randomly skip one or more input pulses or to step more than once for a single input pulse. The cause of this was never determined. Possibly, portions of both circuits were operating at a marginal level, so that a signal periodically failed to switch the next element in the circuit. Or the failure to react could be attributed to a random noise signal that became superimposed on a desired signal in such a way that an OR-NOR element failed to switch off or that it switched on twice for a single command signal. Some random malfunctions of the integrated circuits could also be attributed to possible contaminants that were trapped in or moving through the circuits.

Contamination Problems

The integrated fluidic-controlled stepping-motor actuator system was tested on a newly constructed pneumatic test bench. After initial testing, it became apparent that adequate precautions had not been exercised in cleaning the test bench of possible contaminants. These contaminants were never identified, but failures in the logic of both the counting circuit and the pulse-conditioning circuit of integrated circuit A occurred after limited initial testing. The apparent blockages were removed by flushing the individual amplifiers with high-pressure water or trichloroethane or sometimes with just high-pressure air. During initial tests, integrated circuit B was rendered inoperable by contaminants from the same test bench. The circuit was cleaned by the manufacturer.

After the integrated circuit blockages were freed of contaminants, the bench was reworked to include a 10- to 15-micron sintered metal filter on the bench outputs. A few minor contamination problems again arose with integrated circuit A, but they were probably caused by previously trapped dirt that shifted. There were no further contamination problems with integrated circuit B.

Having the integrated circuit constructed of separable parts, as was done with integrated circuit A, greatly aides in diagnosing circuit malfunctions because each plate can be tested separately. This method of construction also makes the circuit eaiser to clean.

SUMMARY OF RESULTS

Two fluidic integrated circuits, designed to control a pneumatic stepping-motor actuator, were fabricated and tested. Both integrated circuits used the same power amplifiers. From this work the following results were obtained:

1. Through the use of reasonably well-defined procedures for calculating interconnecting passage sizes, an operational breadboard fluidic system can be integrated into a compact self-contained unit.

2. The performance of the fluidic stepping-motor actuator system developed by Lewis was improved. The maximum actuator speed was increased by drilling out the bellows inlet holes to equal the size of the passages in the bellows distribution plate and by increasing the power-amplifier pressure recovery. This increased pressure recovery also produced an increase in output torque over the entire speed range.

3. For developmental testing, it is advantageous to design the integrated circuit in separable modules, which facilitates testing individual components, isolating possible problem areas, and cleaning the circuit if necessary.

4. A desirable method to eliminate contamination problems is to place individual 10- to 15-micron filters in all circuit supply lines.

Lewis Research Center,
National Aeronautics and Space Administration,
Cleveland, Ohio, November 19, 1968,
122-29-03-04-22.

APPENDIX A

SYMBOLS

A	area, in. ² ; cm ²
A, B, C, D	four counting-circuit plates and four corresponding power-amplifier plates
C ₁ , C ₂	amplifier control ports
c	speed of sound, 1100 ft/sec; 3.35×10 ⁴ cm/sec
d	line diameter, in.; cm
g ₀	acceleration due to gravity, 32.2 (lbm)(ft)/(lbf)(sec ²); 8.39×10 ⁻⁴ (kg)(cm)/(N)(sec ²)
L	line length, in.; cm
M	interconnecting passage in pulse-conditioning-circuit plate (delay-line channel)
ṁ	mass flow rate, lbm/sec; kg/sec
Δṁ	change in mass flow rate, lbm/sec; kg/sec
N	interconnecting passage in pulse-conditioning-circuit plate (channel for amplifier 4 output lines, or timing pulses)
O	interconnecting passage in pulse-conditioning-circuit plate (channel carrying output pulses to both sides of each counting-circuit plate)
P	pressure, psia; N/cm ² abs
ΔP	change in pressure, psi; N/cm ² (interconnecting passage pressure drop)
Q	interconnecting passage in counting-circuit interconnecting plate (carry-signal delay-time channel)
R ₁ , R ₂	amplifier receivers
S	supply port
T	command input port (timing pulse)
U	interconnecting passage in counting-circuit plate (carry-signal delay-line channel)
Z _{CO}	transmission-line surge impedance, (lbf/in. ²)/(lbm/sec); (N/cm ²)/(kg/sec)
Z' _{CO}	dimensionless transmission-line surge impedance, normalized with respect to supply pressure and flow of driving amplifier

μ viscosity, (lbf)(sec)/in.²; (N)(sec)/cm²
 ρ density, lbm/cu in.; kg/cu cm
 τ time delay line

Subscripts:

b backward
 C_1, C_2 amplifier control ports
e exhaust
f forward
L line
M, N, O, Q, U interconnecting passages or lines
s supply
x before pulse enters line
y after pulse enters line

APPENDIX B

LINE-SIZING CALCULATIONS

This appendix describes the technique for determining the optimum line sizes used to interconnect circuit elements. Included are calculations and graphs to illustrate the method. The line-sizing technique for simply interconnected amplifiers is completely described in appendix B of reference 2. The technique for determining the size of both the orifice and the delay line of the pulse-conditioning circuit is completely described in appendix C of reference 2.

All interconnecting lines in the integrated circuit were determined by using the single-reflection technique. Use of this technique results in larger line sizes and therefore smaller viscous frictional losses than those in an acoustically terminated line.

Carry-Signal Delay Line

The carry-signal delay line, shown schematically in figure 28, connects the central

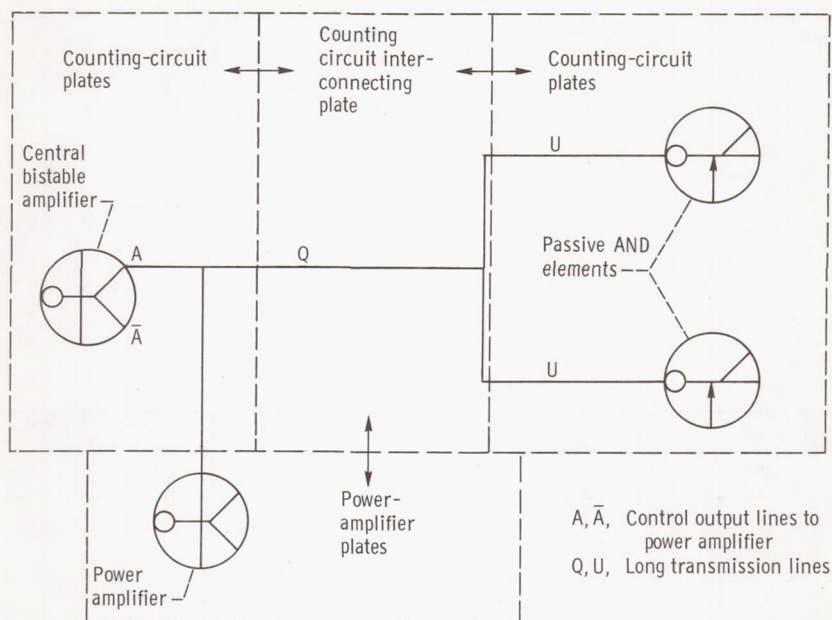


Figure 28. - Carry-signal delay line.

bistable amplifiers with the passive AND elements. The length of the line establishes the delay required prior to resetting the counter circuit. The length varies because of the nature of the integrated construction. The calculated frictional pressure drop was based on the longest line Q, which was approximately 10 inches (25 cm), and the longest line U, which was approximately 10 inches (25 cm).

The load characteristics of the driving amplifier, the central bistable amplifier, are plotted as the solid line in figure 29. Since the central bistable amplifiers also drive the power amplifiers, the control port flow of the power amplifier must be subtracted from the load characteristics of the driving amplifier. The new output load curve is represented by the long-dashed line. Also plotted in this figure are the pressure-flow characteristics of the power nozzles of two OR-NOR gates, which are used as passive AND elements. This figure is normalized with respect to the power nozzle supply pressure and the power nozzle flow of the driving amplifier. Intersection 1 identifies the steady-

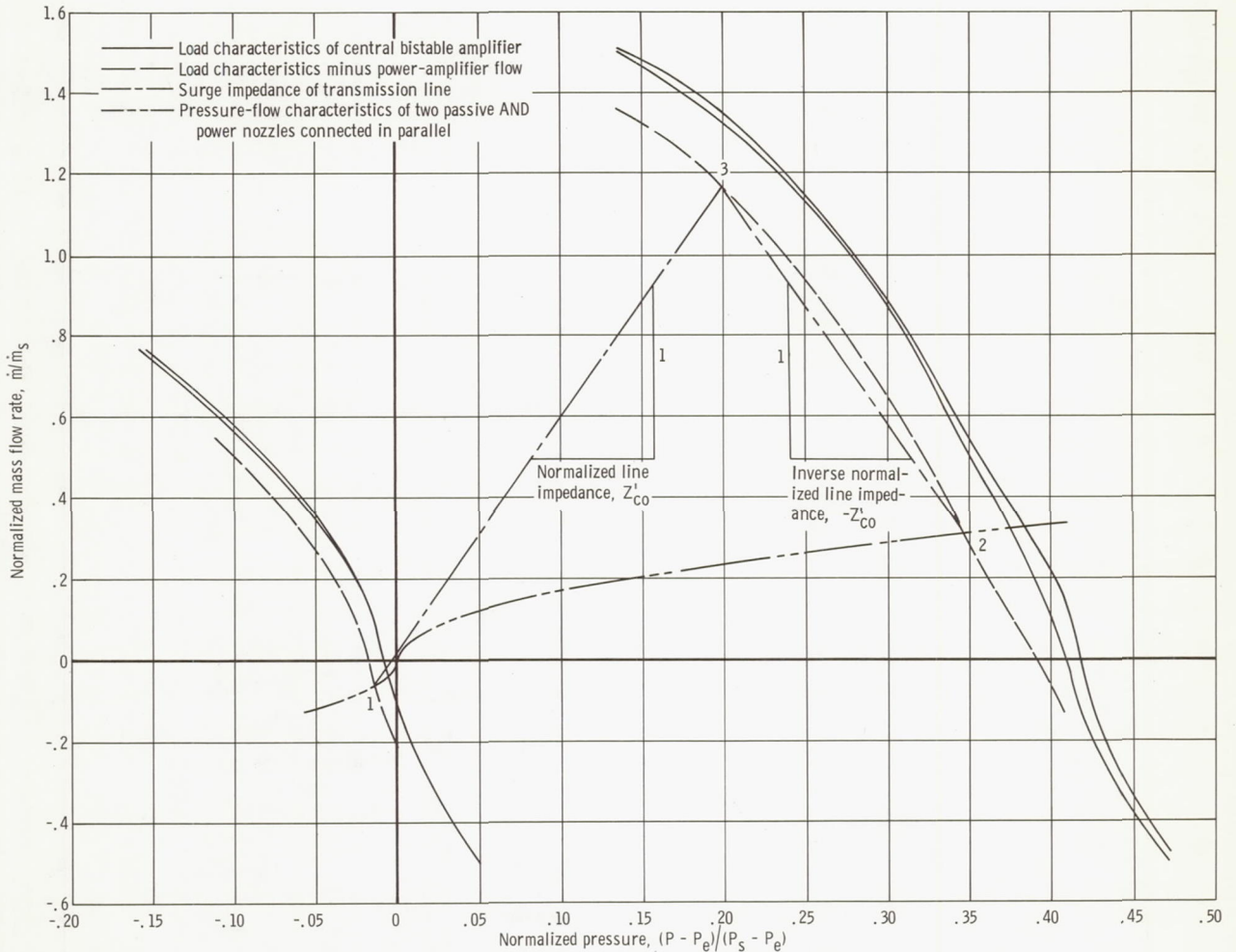


Figure 29. - Determination of size of carry-signal delay line by single-reflection method.

state conditions of the line before the driving amplifier is switched. Intersection 2 identifies the steady-state conditions of the line after the driving amplifier has been switched and all transients have died out. The location of these two steady-state operating points is independent of the surge-line impedance if the frictional losses through the line are considered negligible.

Between these two points the transmission-line dynamics come into play. During the transient after the driving amplifier is switched into the line, the frictionless line initially appears as a resistive impedance Z_{CO} , which is expressed by

$$Z_{CO} = \frac{\rho_y}{\rho_x} \left(\frac{c}{A_L g_0} \right) = \frac{\Delta P}{\Delta \dot{m}} \quad (B1)$$

For most practical cases, the term ρ_y/ρ_x is near 1 and may be neglected. Equation (B1) must be normalized with respect to the power nozzle supply pressure and the supply flow of the driving amplifier before the line impedance can be plotted on the normalized graph:

$$Z'_{CO} = \frac{\Delta P}{P_s - P_e} \frac{\dot{m}_s}{\Delta \dot{m}} = Z_{CO} \frac{\dot{m}_s}{P_s - P_e} \quad (B2)$$

In applying the single-reflection method, a line representing a transmission-line impedance Z'_{CO} is constructed so that a line with an inverse transmission-line impedance $-Z'_{CO}$ will intersect the driving amplifier load characteristics at intersection 2. The first line intersects the load characteristics line at intersection 3. Since the conditions at intersection 3 are not compatible with the pressure-flow characteristics of the terminating impedance, a readjustment of flow conditions at the end of the line is necessary. The pressure at the end of the line must increase, and flow must decrease, which sends a reflected pulse up the line to the driving amplifier. Because the reflected pulse readjusts the flow conditions in the line to the final steady-state value (intersection 3), no further readjustment is necessary. Also, since no further reflections travel down the line to the load, the pulse to the load will be indistinguishable from a pulse delivered to an acoustically matched line.

With the transmission line chosen, the initial pulse sent down the line has a pressure of $0.20(P_s - P_e)$ or 2.4 psig (1.6 N/cm² gage). At the load, the pulse is reflected as a pulse with a final steady-state value of $0.34(P_s - P_e)$ or 4.1 psig (2.8 N/cm² gage).

From the construction in figure 29, the value of the normalized line impedance Z'_{co} was determined to be 0.174. The value for the line impedance Z_{co} was determined from equation (B2) rewritten as

$$Z_{co} = Z'_{co} \left(\frac{P_s - P_e}{\dot{m}_s} \right) \quad (B3)$$

and

$$Z_{co} = \frac{2.17 \times 10^3 \text{ lbf/in.}^2}{\text{lbm/sec}} \left(\frac{3.30 \times 10^3 \text{ N/cm}^2}{\text{kg/sec}} \right)$$

when $Z'_{co} = 0.174$, $P_s - P_e = 12$ psig (8.26 N/cm² gage), and $\dot{m}_s = 0.963 \times 10^{-3}$ pound mass per second (0.436×10^{-3} kg/sec).

Solving for A_L in equation (B1) gives

$$A_L = \frac{c}{Z_{co} g_o} \quad (B4)$$

or for line Q, the area $A_{L,Q}$ is equal to 0.0157 square inch (0.101 cm²).

Line Q splits into two equally sized lines U, each with one-half the area of line Q, or $A_{L,U}$ equals 0.00785 square inch (0.0506 cm²).

The line Q dimensions chosen were 0.125 inch (0.318 cm) wide by 0.125 inch (0.318 cm) deep. Line U dimensions were 0.098 inch (0.249 cm) wide by 0.080 inch (0.203 cm) deep.

The friction losses through the line are determined by

$$\Delta P \cong \frac{128 \dot{m}_L \mu_L L}{\rho_L \pi d_L^4} \quad (B5)$$

The conditions given in the following table were used to calculate the line losses:

	Line	
	Q	U
Length, L, in. (cm)	10.0 (25.4)	10.0 (25.4)
Viscosity, μ_L , (lbf)(sec)/in. ² (N)(sec)/cm ²)	2.6×10^{-9} (1.8×10^{-9})	2.6×10^{-9} (1.8×10^{-9})
Density, ρ_L , lbm/cu ft (kg/cu cm)	0.0953 (0.153×10^{-5})	0.0953 (0.153×10^{-5})
Mass flow, \dot{m}_L , lbm/sec (kg/sec)	0.289×10^{-3} (0.131×10^{-3})	0.144×10^{-3} (0.0653×10^{-3})
Diameter (using round tube of equal area), d, in. (cm)	0.141 (0.358)	0.100 (0.254)

Using these values in equation (B5) results in the following pressure losses:

Line Q:

$$\Delta P_Q = 0.014 \text{ psi } (0.0096 \text{ N/cm}^2)$$

Line U:

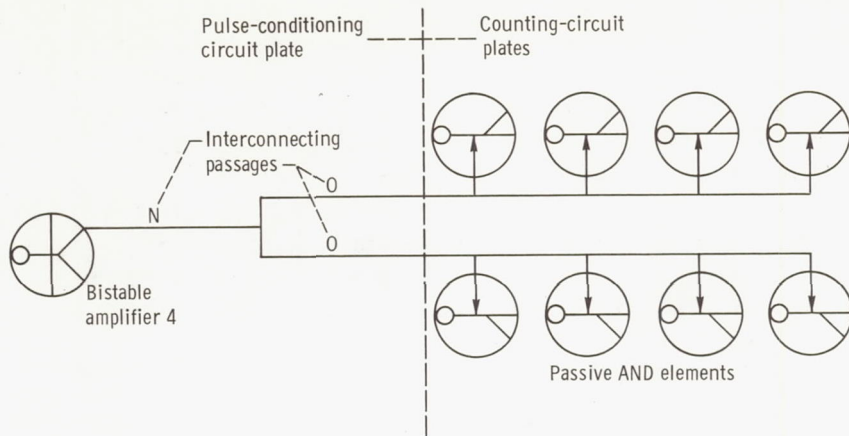
$$\Delta P_U = 0.028 \text{ psi } (0.019 \text{ N/cm}^2)$$

The total pressure loss is 0.042 psi (0.029 N/cm^2). These values are low with respect to the pulse level, 2.4 psig (1.6 N/cm^2 gage), and need not be considered.

Timing-Pulse Line Size

The timing-pulse line connects the pulse-conditioning output, amplifier 4, to the control ports of the eight passive AND elements of the counting circuit. The line with its driving and driven elements are shown in the schematic diagram of figure 30.

The load characteristics of the driving amplifier, amplifier 4 of the pulse-conditioning circuit, are plotted in figure 31. Also plotted are the pressure-flow characteristics of the combined control ports of the eight OR-NOR gates used as passive AND elements. The characteristics are normalized with respect to the power nozzle supply pressure and power nozzle flow of the driving amplifier. Because the supply pressures and the power nozzle areas of the driving and driven amplifiers are different, scaling



CD-10147-03

Figure 30. - Timing-pulse line.

factors must be used when the normalized characteristics of one amplifier are plotted on the normalized characteristics of the other. The scaling factors are

$$\frac{(P_s - P_e)_{\text{driving}}}{(P_s - P_e)_{\text{driven}}} = 2.5$$

and

$$\frac{\dot{m}_{s, \text{driving}}}{\dot{m}_{s, \text{driven}}} = 0.78$$

The normalized control port pressure and flow characteristics of the driven elements must be divided by these factors when they are plotted on the normalized output characteristics of the driving element.

The single-reflection normalized line impedance Z'_{CO} was determined from figure 31 to be 0.207. The line impedance Z_{CO} was determined by equation (B3) to be

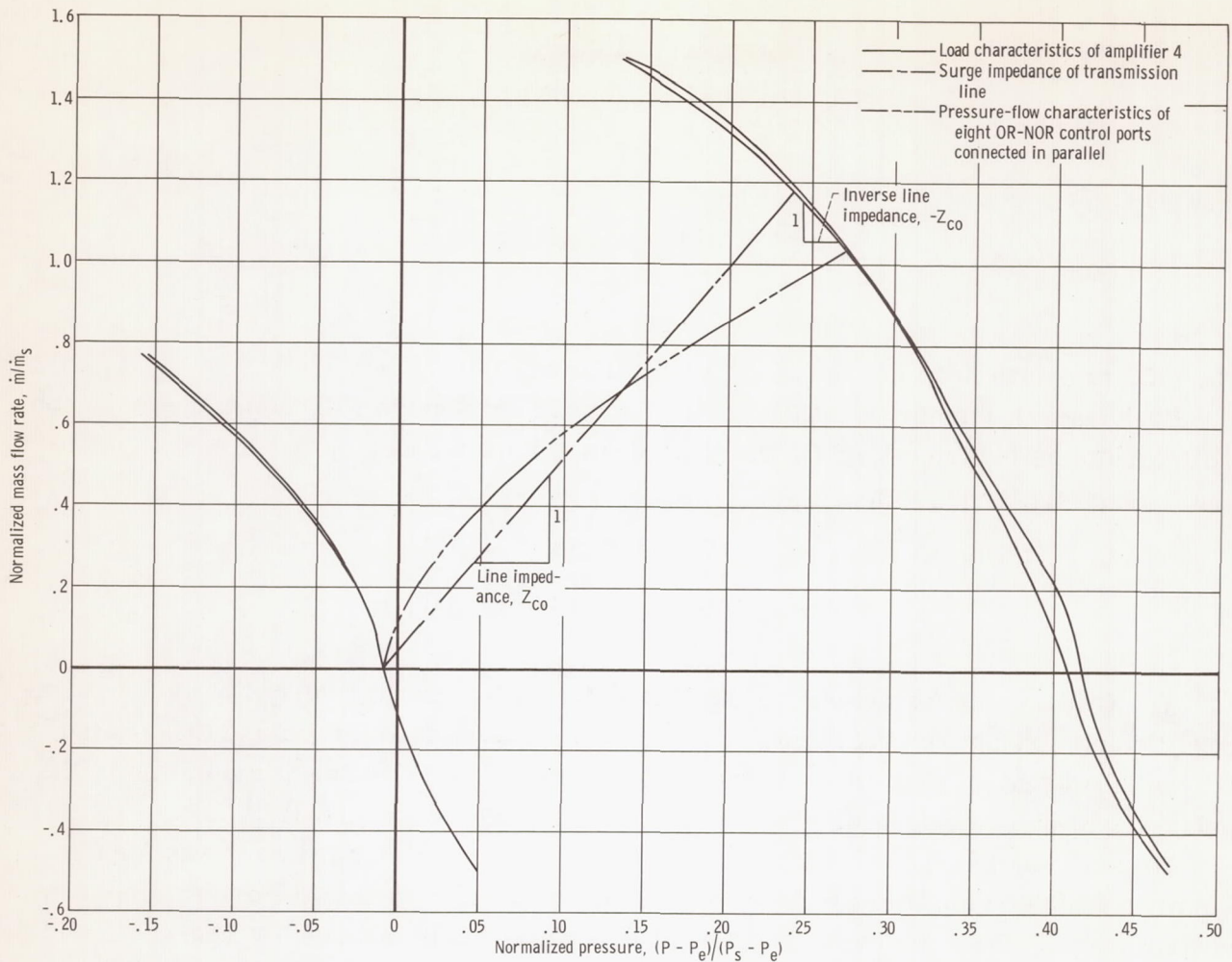


Figure 31. - Determination of size of timing-pulse line by single-reflection method.

2.29×10^3 pounds force per square inch per pound mass per second ($(3.48 \times 10^3 \text{ N/cm}^2)/(\text{kg/sec})$).

The line N area $A_{L,N}$ was determined from equation (B4) to be 0.0149 square inch (0.0960 cm^2), and the line O area $1/2 A_{L,N}$ was calculated to be 0.0075 square inch (0.0484 cm^2). Dimensions used for line N were 0.130 inch (0.330 cm) wide by 0.115 inch (0.292 cm) deep, and those for line O were 0.094 inch (0.239 cm) wide by 0.080 inch (0.203 cm) deep.

The length of line N is 1.50 inches (3.81 cm), and that of line O is 1.50 inches (3.81 cm). When these values were used in equation (B5), the following frictional pressure drops were determined:

Line N:

$$\Delta P_N = 0.0084 \text{ psi (0.0058 N/cm}^2\text{)}$$

Line O:

$$\Delta P_O = 0.017 \text{ psi (0.012 N/cm}^2\text{)}$$

The total pressure drop was 0.025 psi (0.017 N/cm²).

Each line O terminates at the control port of four passive AND units. As each control port line is fed from line O, the area of the line is reduced by 25 percent to maintain the correct termination.

Pulse-Conditioning-Circuit Design

The calculations for determining the size of the orifice and the delay line in the pulse-conditioning circuit are presented in this section. The method for making these calculations is presented in detail in appendix C of reference 2. A schematic diagram of the pulse-conditioning pulse-width-fixation elements is shown in figure 32.

Determining the size of delay line M is not as straight forward as it was for the simply connected amplifiers because of changing pressures in both the driven amplifiers control ports. When one control port is pressurized, the pressure-flow characteristic of the opposite control port is changed because of control port crossflow. An input orifice can be designed to switch the amplifier 3 output to receiver R₂ when control port C₂ is open to the atmosphere. Also, a delay-line diameter can be calculated which will switch amplifier 3 back to receiver R₁ when control port C₁ is open to the atmosphere. However, because control port C₁ is not open but is actually pressurized, the pulse delivered to control port C₂ may not be of the proper shape and amplitude to provide reliable switching back to receiver R₁.

To account for the effects of control port crossflow, it is necessary to obtain a plot of the pressure-flow characteristics of both the driving amplifier receiver and the driven amplifier control port as a function of the opposite control port pressure.

The following procedure was used to determine the input orifice diameter and the delay-line area. This procedure is an iterative process because an initial output pressure must be assumed for amplifier 2. The following steps show the calculations of the final iteration of the procedure.

Step 1. - An inlet orifice diameter of 0.022 inch (0.056 cm) and an initial pulse height on the output of amplifier of 0.84 psig (0.58 N/cm² gage) were assumed. The out-

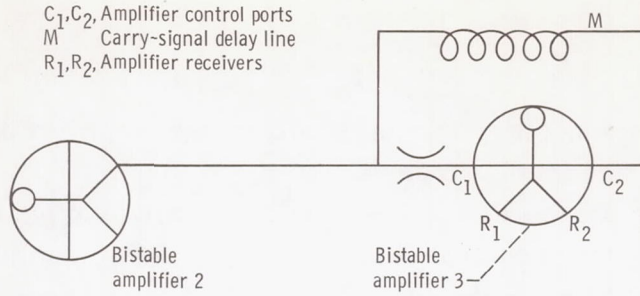


Figure 32. - Pulse-conditioning pulse-width-fixation elements.

CD-10148-03

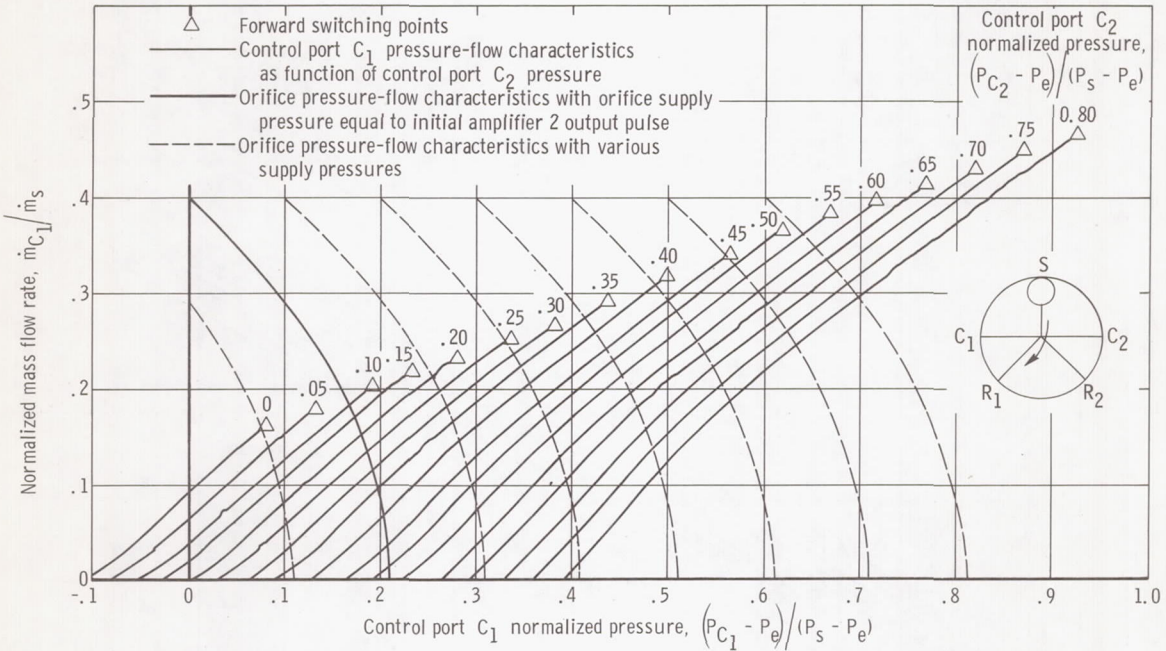


Figure 33. - Determination of combined orifice control port pressure-flow characteristics of amplifier 3 when switched to receiver R_1 .

put pressure-flow characteristics of the orifice are plotted in figure 33 (the heavy solid line crossing the unswitched amplifier 3 control port characteristics). This characteristics curve crosses the zero pressure line of $(P_{C_2} - P_e)/(P_s - P_e)$ well above the switching pressure of $(P_{C_1} - P_e)/(P_s - P_e)$ at $0.080 (P_s - P_e)$. This position indicates that, with the orifice diameter selected, the initial pulse will switch amplifier 3 to receiver R_2 when amplifier 2 is switched into its receiver R_1 .

Step 2. - The orifice pressure-flow characteristics are also plotted in figure 34 as a heavy solid line on the switched control port characteristics of amplifier 3. This plot defines the pressures and flows at the control port C_1 for various control port C_2 pressures and a fixed amplifier 2 output pressure of 0.84 psig (0.58 N/cm^2 gage).

Step 3. - The heavy solid-line curves plotted in steps 1 and 2 in figures 33 and 34 define the combined orifice control port C_1 pressure-flow characteristics for only one value of amplifier 2 output pressure, 0.84 psig (0.58 N/cm^2 gage). The combined characteristics at all amplifier 2 output pressures are determined by shifting the orifice pressure-flow curve sideways both plots. These new curves are the dashed lines in

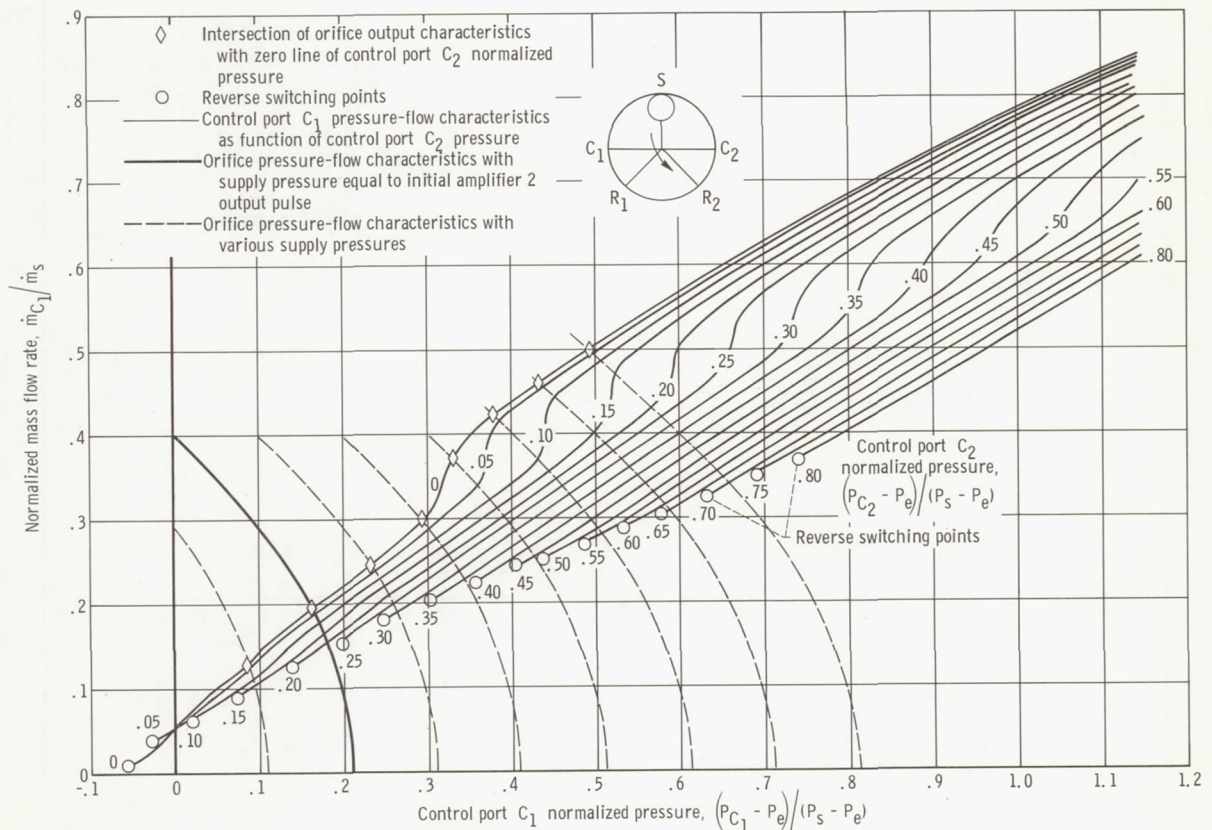


Figure 34. - Determination of combined orifice control port pressure-flow characteristics of amplifier 3 when switched to receiver R_2 .

figures 33 and 34. The procedure is equivalent to changing the orifice upstream pressure. The assumption is that, in the range of pressures considered, the fluid upstream density does not change; therefore, the shape of the curve does not change. The intersections of the orifice output characteristics with the line $\left(\frac{P_{C_2} - P_e}{P_s - P_e}\right) = 0$ (fig. 34) are represented by diamond shaped symbols. The flows at these intersections and the pressures at which the orifice characteristics lines cross the horizontal pressure axis determines the flow consumed by the orifice control port C_1 as a function of amplifier 2 output pressure. This relation will be used in step 5 to determine the initial pressures and flows available to drive the delay line.

Step 4. - If amplifier 3 is assumed to be symmetrical, the characteristics of control port C_1 (shown in figs. 33 and 34) can also be used to represent the characteristics of control port C_2 . The subscripts 1 and 2 are merely interchanged. These curves are shown in figures 35 and 36. The orifice pressure-flow plot for the initial amplifier 2 pressure (heavy solid line in figs. 33 and 34) can now be cross plotted to figures 35 and 36. Figure 33 was used to plot the curve of figure 36, and figure 34 was used to plot the curve of figure 35. The plots thus obtained represent the characteristics of control port C_2 when amplifier 2 output pressure is the initially assumed value of 0.84 psig (0.58 N/cm² gage).

Step 5. - The pressure-flow characteristics of control port C_2 , as determined in step 4, are plotted on the amplifier 2 load characteristics in figure 37. The load characteristics of amplifier 2 must be altered to allow for the flow consumed by the orifice. The load characteristic curve with the orifice flows subtracted is shown as a long dashed line. No scaling is required in constructing these plots because the supply pressures and power nozzle size of both amplifiers is the same.

The control port characteristics line crosses the equivalent amplifier 2 load characteristics at $0.35 (P_s - P_e)$. This point corresponds to 1.4 psig (0.96 N/cm² gage) which is sufficient pressure to reset amplifier 3.

The delay-line surge impedance Z'_{CO} can be determined by drawing a line between the initial condition of the delay line (point A) and the intersection of the initial assumed orifice pressure with the equivalent amplifier 2 load characteristics (point B). The delay-line surge impedance cannot be arbitrarily chosen as was done when the carry-signal and timing-pulse lines were sized. The surge impedance of the delay line is specified by the initial pressure and flow in the line before amplifier 2 is switched (point A) and by the initial pressure and flow that result when amplifier 2 is switched into it (point B). These points were chosen at the beginning of the iteration process to size the input orifice.

Since the final pressure and flow, which satisfy both the control port characteristics of amplifier 3 and the load characteristics of amplifier 2, at point C, there must be a readjustment of conditions in the line. A reflection will therefore travel back to the out-

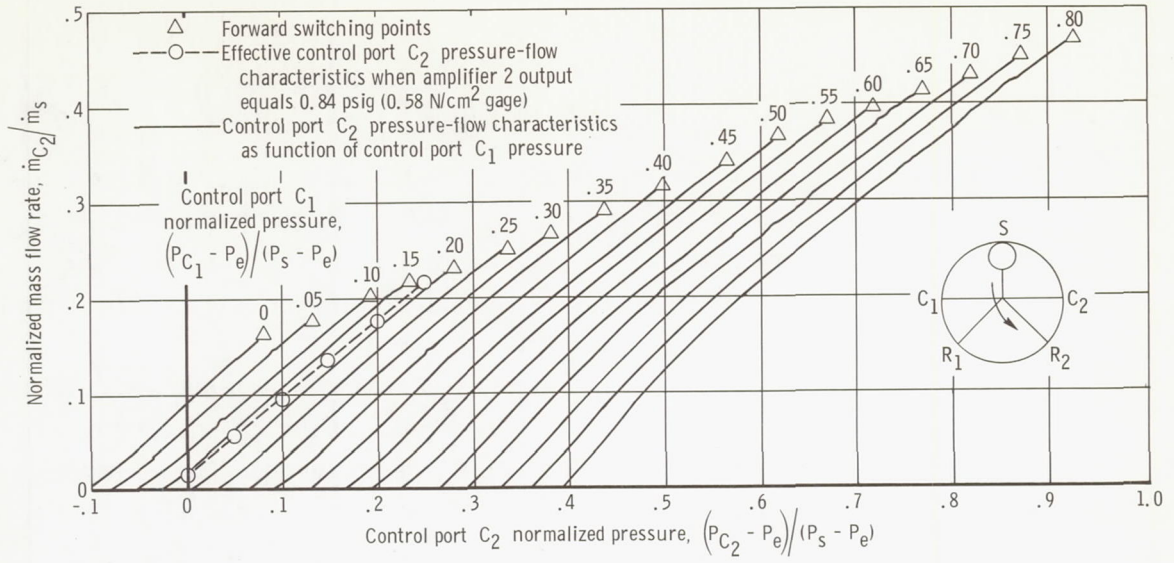


Figure 35. - Effective pressure-flow characteristics of amplifier 3 control port C_2 when switched to receiver R_2 .

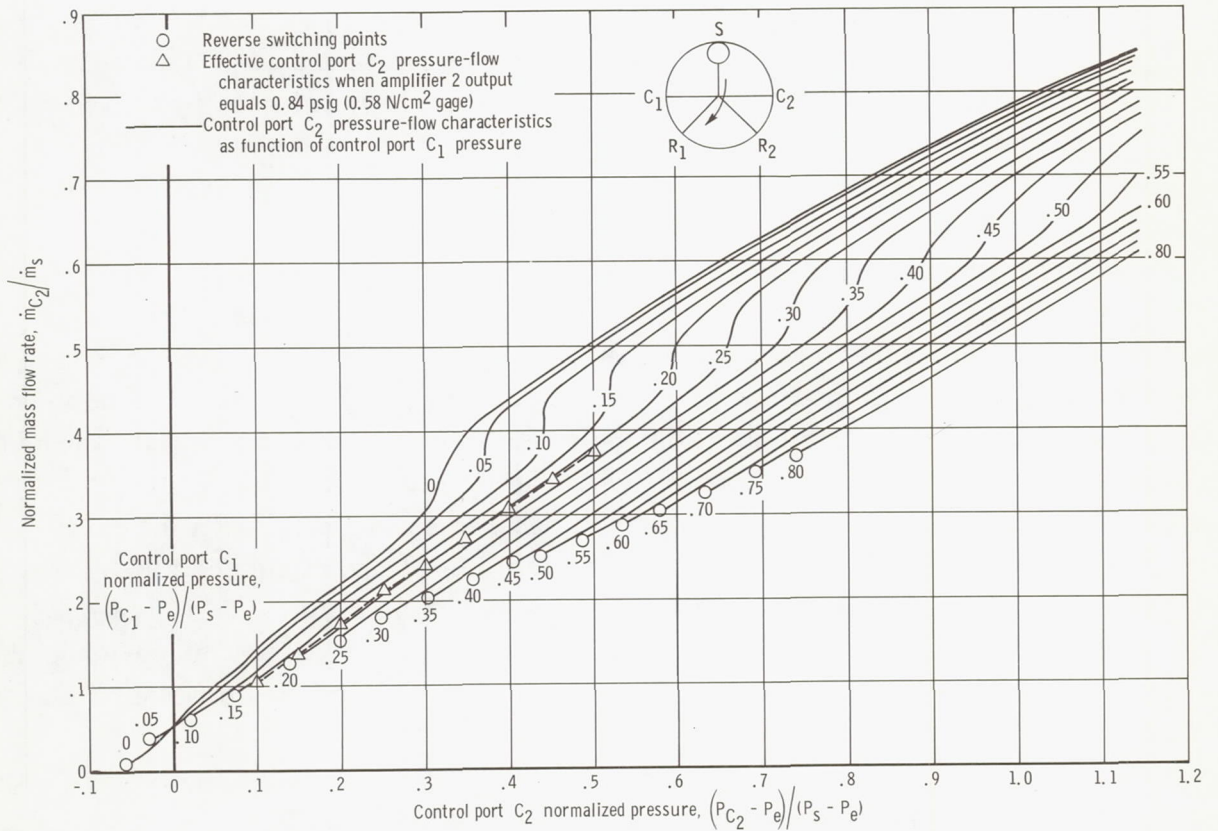


Figure 36. - Effective pressure-flow characteristics of amplifier 3 control port C_2 when switched to receiver R_1 .

put of amplifier 2. A line drawn from point B at a slope of $-Z_{CO}$, to intersect the line of the control port characteristics of amplifier 3, determines the magnitude of the re-
 flected pulse pressure and flow. This intersection is point D in figure 37. The delay
 line thus sized is nearly a single reflection line.

From figure 37 the line surge impedance was determined to be 0.55×10^4 pounds
 force per square inch per pound mass per second ($(0.836 \times 10^4 \text{ N/cm}^2)/(\text{kg/sec})$). The
 line area calculated from equation (B4) was 0.0062 square inch (0.040 cm^2). The line
 dimensions selected were 0.077 inches (0.19 cm) wide by 0.080 inch (0.20 cm) deep.
 The delay-line friction losses, calculated with equation (B5), were 0.066 psi (0.045
 N/cm^2). This amount of loss is considered negligible.

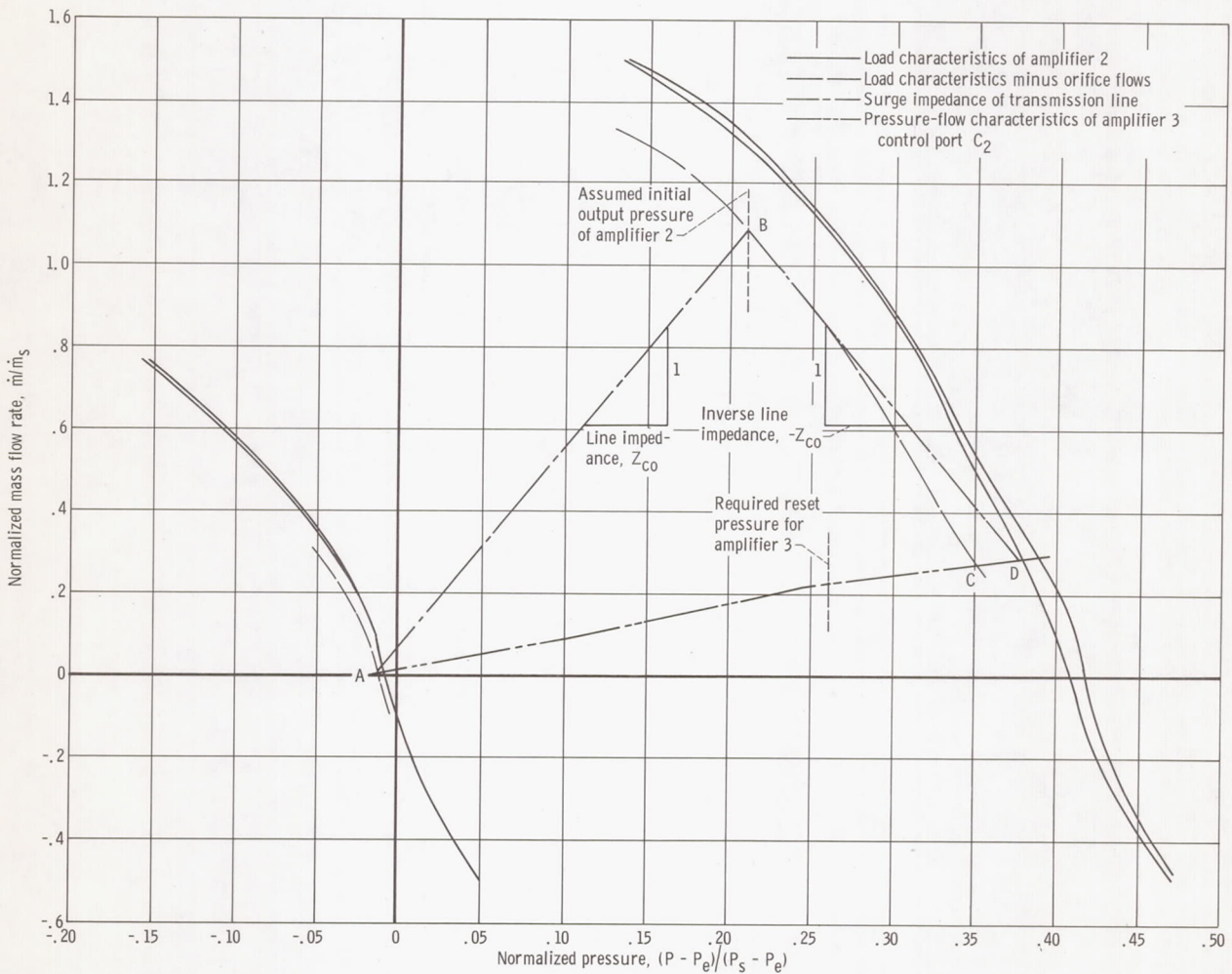


Figure 37. - Determination of pulse-conditioning delay-line size.

REFERENCES

1. Howland, G. R. : Pneumatic Nutator Actuator Motor. Rep. BPAD-863-16719R, Bendix Corp. (NASA CR-54788), Oct. 17, 1965.
2. Griffin, William S. : A Breadboard Fluoric-Controlled Pneumatic Stepping Motor System. NASA TN D-4495, 1968.